37. CRYSTAL MORPHOLOGIES AND PYROXENE COMPOSITIONS IN BONINITES AND THOLEIITIC BASALTS FROM DEEP SEA DRILLING PROJECT HOLES 458 AND 459B IN THE MARIANA FORE-ARC REGION[1]

James H. Natland, Deep Sea Drilling Project, Scripps Institution of Oceanography, La Jolla, California

ABSTRACT

Not all boninites are glassy lavas. Those of Hole 458 in the Mariana fore-arc region are submarine pillow lavas and more massive flows in which glass occurs only in quenched margins. Pillow and flow interiors have abundant plagioclase spherulites, microlites, or even larger crystals but can be recognized as boninites by (1) occurrence of bronzite, (2) presence of augite–bronzite microphenocryst intergrowths, and (3) reversal of the usual basaltic groundmass crystallization sequence of plagioclase–augite to augite–plagioclase. The latter is accentuated by sharply contrasting augite and plagioclase crystal morphologies near pillow margins, a consequence of rapid cooling rates. This crystallization sequence appears to be a consequence of boninites having higher SiO_2 and $Mg/Mg + Fe$ than basalts but lower CaO/Al_2O_3.

Microprobe data are used to illustrate the effects of rapid cooling on the compositions of pyroxene and microphenocrysts in a glassy boninite sample and to estimate temperatures of crystallization of coexisting bronzite and augite. A range from 1320°C to 1200°C is calculated with an average of 1250°C. This is higher by 120°–230° than the known range for western Pacific arc tholeiites and by over 300° than for calc–alkalic andesites.

Boninites of Hole 458 lack olivine and clinoenstatite but are otherwise chemically and petrographically similar to boninites that have these minerals. In order to distinguish the two types, the Hole 458 lavas are here termed *boninites* and the others are termed *olivine boninites*.

Arc tholeiite pillow lavas from Holes 458 and 459B are briefly described and their textures compared to fractionated, moderately iron-enriched, abyssal tholeiites. Massive tholeiite flows contain striking quartz–alkali feldspar micrographic intergrowths with coarsely spherulitic textures resulting from *in situ* magmatic differentiation. Such intergrowths are rare in massive abyssal tholeiites cored by DSDP and probably occur here because arc tholeiites have higher normative quartz at comparable degrees of iron enrichment—a result of higher oxygen fugacities and earlier separation of titanomagnetite—than abyssal tholeiites.

INTRODUCTION

This chapter describes crystal morphologies and textures of lavas recovered from Holes 458 and 459B of the Mariana fore-arc region during Deep Sea Drilling Project Leg 60 (Fig. 1). The majority of lavas in Hole 458 are chemically and petrographically distinct members of what has been termed the *boninite series* by Bloomer et al. (1979) and Meijer et al. (this volume). The lavas were extruded as pillows and massive flows onto the seafloor and consequently have a considerable range in crystallinity, with great differences in the sizes and shapes of crystals from sample to sample. The recovery of an extensive suite of these lavas from Hole 458 allows them to be described in a more comprehensive manner than has previously been attempted; the principal objective is to relate glassy samples to more coarsely crystalline samples from pillow interiors and massive flows. Also occurring in both holes are tholeiitic basalts with the chemical characteristics of island arc tholeiites (Wood et al., this volume). These also were extruded as pillows and massive flows and, although more altered than the boninite series lavas, can be described in much the same way. The descriptions may be of interest to those who wish to compare these lavas with subaerial equivalents or abyssal tholeiites.

BACKGROUND

The recovery of boninite series lavas from Hole 458 was one of the most significant results of Leg 60. At the time of the drilling, petrologists were just begining to be aware of the role of these rocks in island arc magmatism (e.g., Kuroda and Shiraki, 1975). Boninites had been named and described as early as the late 19th century (Kikuchi, 1888, 1890; Petersen, 1891) but remained little more than a curiosity among rock types for almost 90 years. Dallwitz et al. (1966) described clinoenstatite-bearing lavas from the Cape Vogel area of Papua, but mainly to emphasize their unusual mineralogy. These lavas are now recognized to be boninites (Cameron et al., 1980). Although Dietrich et al. (1978) described boninites from dredge hauls in the Mariana Trench, they identified the suite as originally ocean crust because the boninites occurred in an "ophiolitic" assemblage of pillow basalts, dolerites, gabbros, and ultramafic rocks. Only a combined study of the Bonin Islands (Kuroda and Shiraki, 1975; Shiraki and Kuroda, 1975, 1977; Kuroda et al., 1978; Shiraki et al., 1977, 1978) and Leg 60 drilling have prompted the general realization that these are island arc lavas (e.g., Meijer, 1980; Cameron et al., 1979, 1980; Sharaskin et al., 1980).

The evidence that the lavas from Hole 458 are island arc lavas is that arc-derived turbidites began draping the entire fore-arc region, including the pillow lavas of Holes 458 and 459B, in the late Eocene–early Oligocene

[1] *Initial Reports of the Deep Sea Drilling Project*, Volume 60.

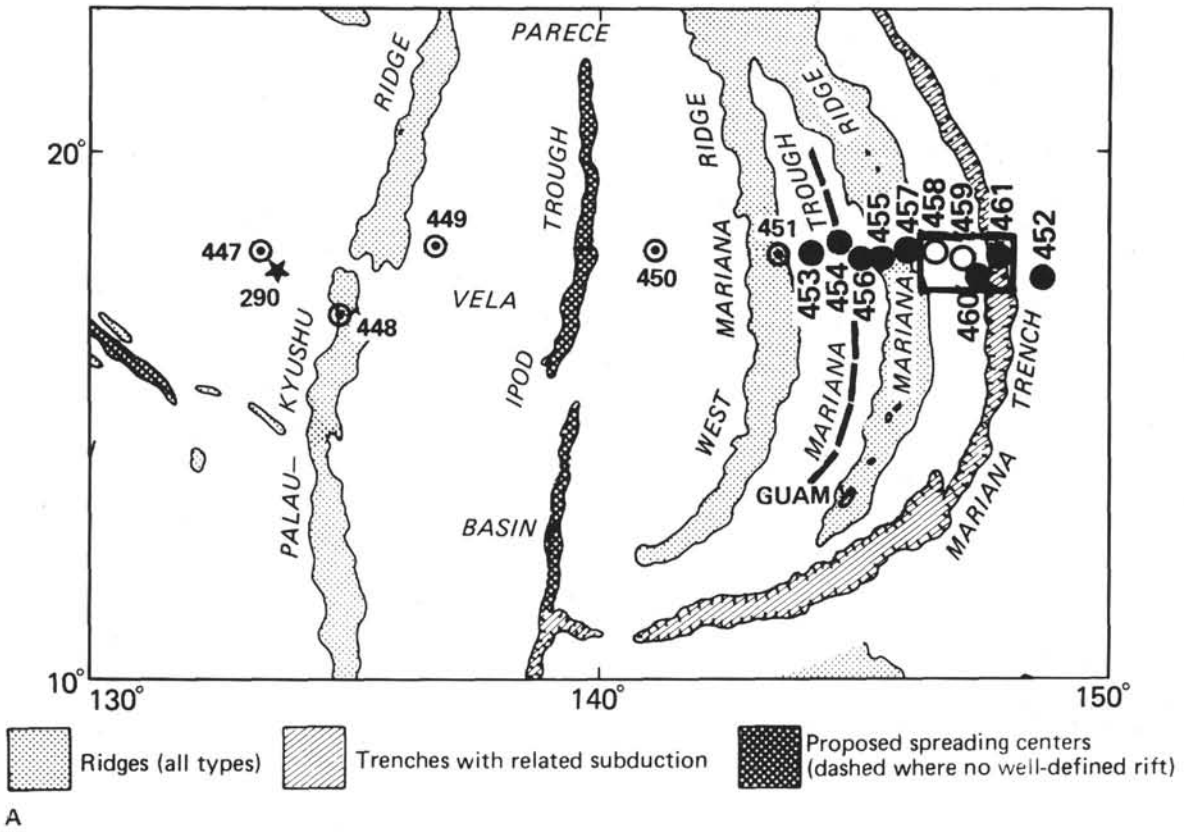

A

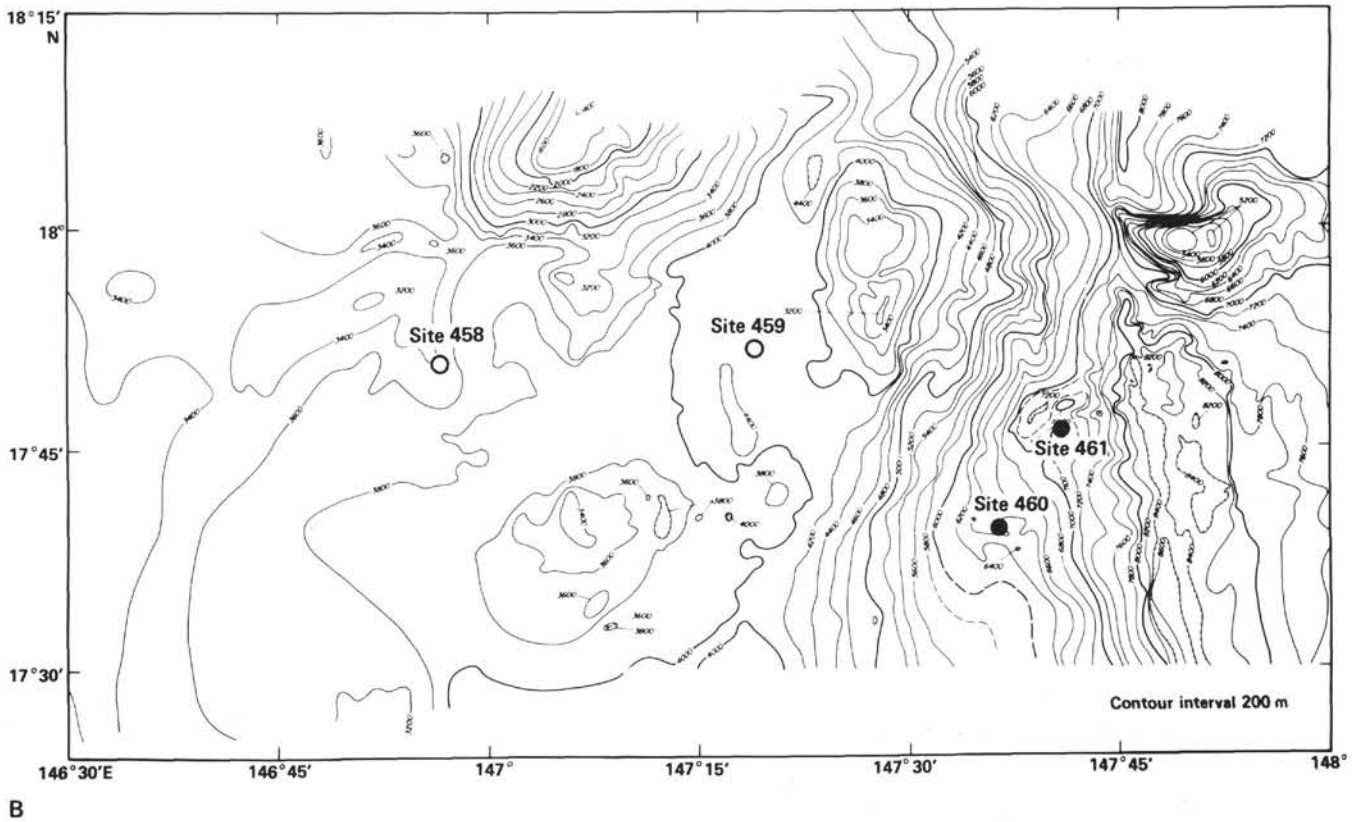

B

Figure 1. A. Location of Sites 458 and 459 (open circles) in the Mariana fore-arc region. Other Leg 60 sites are closed circles. Leg 59 sites are circled dots. Site 290 (Leg 31) is shown by a star. The box encloses area of B, bathymetry of the fore-arc and trench region near Sites 458 and 459, from Hussong and Fryer (this volume). Contour interval is 200 meters.

(see reports for Sites 458 and 459, this volume). Moreover, basalts associated with the boninite series lavas in Hole 458 and all the lavas of Hole 459 have island arc tholeiite compositions (Wood et al., Meijer et al.; Sharaskin; Bougault et al.; Hickey and Frey, all this volume). Additionally, island arc tholeiites and a boninite-type rock were recovered at Sites 460 and 461 in the Mariana Trench in talus beneath Eocene sediments (see Sites 460 and 461 reports; Meijer et al.; Sharaskin, all this volume). The fore-arc basement is thus of island arc composition, as old as the oldest lavas on Guam and Saipan (Schmidt, 1957; Stark, 1963), and probably crops out in fault exposures in the trench wall. Cameron et al. (1980) have described boninite occurrences in the Troodos, as well as other ophiolites, and postulate that ophiolites containing boninites originate in tensional environments either at the onset of subduction or at a time of sudden change in the direction of plate motion. Natland and Tarney (this volume) suggest that the top of basement in Holes 458 and 459B is the potential upper part of an *in situ* ophiolite succession, one which originated not as ocean crust but in an island arc setting.

Apart from these tectonic considerations, boninites and related rocks have compositions, mineralogies, and textural features of no little theoretical interest. Chemically, they typically have high SiO_2 (52–58%) coupled with high MgO (9% or more), as well as several hundred parts per million apiece of Cr and Ni, but low TiO_2 (0.2–0.5%) and Zr (20–40 ppm). Glassy boninites usually have a fair amount ($\sim$5%) of dissolved water (e.g., Cameron et al., 1979; Meijer, 1980). These features suggest that the rocks are derived by partial melting of a hydrous peridotite, as indicated by experimental data (O'Hara, 1965; Kushiro, 1969, 1972a, 1974; Mysen et al., 1974; Green, 1976). Of great interest has been the occurrence in some boninites of clinoenstatite (Dallwitz et al., 1966; Dietrich et al., 1978; Komatsu, 1980). Prior to the descriptions of Dallwitz et al. (1966), terrestrial examples of lavas demonstrating the inversion of proto- to clinoenstatite were unknown, even though clinoenstatite had been produced experimentally by stressing enstatite (Turner et al., 1960) and phase relationships had been determined establishing that clinoenstatite could form metastably by cooling protoenstatite through the protoenstatite $\rightleftarrows$ orthoenstatite inversion (Boyd and Schairer, 1964; Brown, 1968, 1972; Nakamura, 1971; Mori, 1978). As a consequence of the latter, there has been a general recognition that the occurrence of clinoenstatite in these siliceous glassy rocks reflects not only their unusual compositions but also the high cooling rates they had undergone.

One difficulty in identifying boninites and related rocks stems from the original definition of the term. Petersen (1891) named boninites on the basis of both their characteristic mineral assemblages and their unusual composition. Johannsen (1937) defined boninite as glass-rich, nearly feldspar-free olivine–bronzite andesite with phenocrysts of olivine, bronzite, and augite. Recently, Cameron et al. (1979) redefined boninite as "a highly magnesian but relatively siliceous glassy rock containing one or more varieties of pyroxene, some or all of which have a morphology characteristic of rapid growth, accessory magnesiochromite, and, commonly, minor amounts of olivine. Laths of amphibole or plagioclase microlites are rare" (p. 550).

Despite these definitions, it is still difficult to identify the Hole 458 lavas as boninites. The chief differences between these lavas and the material in the definitions are that the glassy Hole 458 lavas lack olivine and clinoenstatite—although that does not seem to be crucial. Magnesiochromite is also very rare, whereas it is quite abundant in olivine-bearing boninites. The most important difference is that few of the Hole 458 lavas are glassy. The majority contain abundant spherulitic to microlitic plagioclase, and many have intersertal and even subophitic textures in which plagioclase is a dominant mineral.

The explanation for the lack of olivine and clinoenstatite seems to be that the Hole 458 lavas are somewhat fractionated. Kushiro (this volume) determined that two samples from Hole 458 he examined experimentally could not have melted in equilibrium with a hydrous peridotite mantle, unlike boninites previously investigated; instead, they had a more magnesian boninite parent which experienced fractionation of olivine and enstatite. Meijer (1980), noting the lower magnesian composition of the Hole 458 lavas compared with typical boninites but recognizing their obvious general compositional similarities, proposed the existence of a boninite series, analogous in certain respects to the island-arc-tholeiite and calc–alkalic magma series of island arcs (this had been proposed earlier by Bloomer et al., 1979). He defined boninite series on normative criteria rather than on mineralogy.

But even broadening the definition of boninites in this way to include the Hole 458 lavas does not confront the problem of contrasting conditions of crystallization of these lavas, whether they are rigorously boninites or not. It is unusual in the history of petrography for the definition of a mafic rock to be based on the characteristics of glassy, rapidly quenched lavas. Pillow basalts are commonly glassy only in their outermost few centimeters, and these lavas are no different. It is to be expected then that the vast majority of pillowed boninites (or high-MgO bronzite andesites) will be far more crystalline in the interior than in the narrow exterior glassy rind. But by the petrographic definitions just cited, even the interiors of small pillows could not be termed boninites because they usually lack glass. Should the same lava composition erupt on land, there would be little or no glassy outer margin. Obviously, any proper petrographic identification of subaerial boninite must be based on descriptions of lavas cooled more slowly than pillow margins.

In this chapter, then, a principal objective will be to outline the crystallization of the Hole 458 boninite series lavas through the entire range of cooling rates and undercooling represented by pillow rims, pillow interiors, and massive flows. From this, reliable criteria for identifying boninite-series lavas among coarser grained rocks can be stated. Certain features in the glassy lavas do not occur in the more coarsely crystalline rocks.

Electron microprobe analyses of minerals will be used to show that these features are the consequence of rapid quenching at pillow margins. Pyroxene compositions will be used to estimate temperatures of crystallization of the lavas. This done, the general problem of boninite series classification will be considered. Finally, the petrographic features of associated tholeiitic basalts will be described. These have some geochemical features, such as iron enrichment, that are reminiscent of abyssal tholeiites, to which they will be compared.

This chapter is the third in a series of mine devoted to crystal morphologies of submarine lavas recovered by the Deep Sea Drilling Project and is the first to deal with island arc lavas. The basic concept of the previous two papers (Natland, 1978, 1980) will be followed here. My premise is that undercooling is most extreme at cooling unit boundaries (where crystallization is suppressed to such an extent that glass forms) and least in the interiors and that one may therefore trace modifications in crystal morphologies and increasing crystallinity literally from the outside of cooling units into the interior as an approximate function of decreasing undercooling. The foundations for such an approach were laid by Kirkpatrick (1978), following experimental verification that a wide range of crystal morphologies of plagioclase (Lofgren, 1974) and olivines (Donaldson, 1976) can be related systematically to undercooling. The boninite series lavas of Hole 458, however, are striking in that pyroxene assumes much of the role that plagioclase does in basalts in the development of rock textures, and some features of pyroxene microphenocrysts have no experimental or natural analog among olivines or plagioclases. These will be pointed out as they are discussed. Apart from these unusual occurrences, I will use the terminology of Lofgren (1971, 1974) and Donaldson (1976) for crystal morphologies and spherulitic forms in general.

BASEMENT LITHOLOGIES AND COMPOSITIONS IN HOLES 458 AND 459B

Lithologic representations of basement, identification of the principal chemical types and subtypes based on data of Wood et al. (this volume), and summary magnetic stratigraphies for Holes 458 and 459B are shown in Figure 2. The two basic chemical types in both holes are designated A, for boninite series lavas, and B, for basalts. Subtypes are identified by numerical subscripts. Average chemical analyses and CIPW norms are listed in Table 1. There are two intervals of boninite series lavas in Hole 458, comprising Lithologic Units 1, 2, 3, and part of 4. The abrupt change in magnetic inclinations between Lithologic Units 3 and 4 was probably the result of a reversal in the Earth's magnetic field between the times these two units were extruded (Bleil, this volume; Natland and Tarney, this volume). Within the boninite series lavas, Lithologic Units 1 and 3 are mainly pillows; Lithologic Unit 2 is a pair of fairly massive flows. Lithologic Units 4 and 5 are pillows and thin flows.

The boninite series lavas of Lithologic Unit 4 differ compositionally from those of Units 1–3 (Table 1), having more TiO_2 and Zr at a given abundance of MgO (Wood et al., this volume; Bougault et al., this volume). Within Chemical Type A_1 (Lithologic Units 1–3) there is some chemical variation, but TiO_2 abundances are so low (less than 0.4%) that this normally sensitive discriminant is useless for defining chemical units. Most other major oxides are either poorer discriminants or are highly mobile during alteration, which is locally extensive. Most of the lavas have MgO contents between 5% and 7%. Those intervals with MgO greater than 8% in reasonably fresh samples are indicated by brackets to the right side of the lithologic column (Fig. 2). Samples from the upper flow of Lithologic Unit 2 have unusually high SiO_2 (57–59%) coupled with low MgO (4.5–5.5%) leading to high normative quartz (8–10%; see Table 1). It seems likely therefore that Chemical Type A_1 consists of several chemical subtypes, but their boundaries have been obscured by alteration (see Site 458 report, this volume).

Hole 459B consists of two major basaltic subtypes, B_1 and B_2, which differ in that B_1 has higher MgO contents and lower $Fe_2O_3^T$ contents than B_2. Still finer compositional subtypes can be defined on the basis of small chemical differences (see Table 2 and Site 459 Report, this volume). Subtype B_{1A} is actually compositionally very similar to Subtype A_2 of Hole 458 but consists of flows rather than glassy pillows and lacks orthopyroxene; hence it was not identified as belonging to the boninite series. Alteration in Hole 459B is more extensive than in Hole 458 and could very well have destroyed any orthopyroxene phenocrysts present.

The various B_2 subtypes in Figure 2 show variable enrichment in $Fe_2O_3^T$ and TiO_2. This apparently influenced the formation of abundant titanomagnetite in the lavas, producing high intensities of magnetization (Bleil, this volume). The two most iron-enriched lavas are B_2 of Hole 458 and B_{2A} of Hole 459B. Both have over 13.5% $Fe_2O_3^T$ (Table 1; see discussion in Natland and Tarney, this volume).

Petrography of Hole 458 Boninite Series Lavas

Because of the extensive alteration, the outer, glassiest parts of boninite series pillows were not recovered in Hole 458. Those samples which appear to have been closest to the outer edges of pillows occur in Lithologic Unit 3 (Chemical Type A_1) and are fairly altered. They contain abundant clinopyroxene spherulites that usually consist of small crystals surrounded by dense overgrowths of tiny fibers in pale brown glass (Fig. 3A). Many of the small crystals have fibers attached mainly from their ends. In rocks that crystallized at slightly lower cooling rates (farther into pillows), these fibrous attachments are shorter and less pronounced (Fig. 3B). In still other glassy rocks, acicular rather than spherulitic clinopyroxene microlites are well developed (Fig. 3, C–F). These occur mainly near the top of Lithologic Unit 1 (Type A_1). In these rocks, there are also brown spherulites (Fig. 3, C and D) that contain sworls of needlelike plagioclase and abundant vesicles. These are the only places where vesicles occur in the glassy samples. Within about 1 cm of the outermost portions of

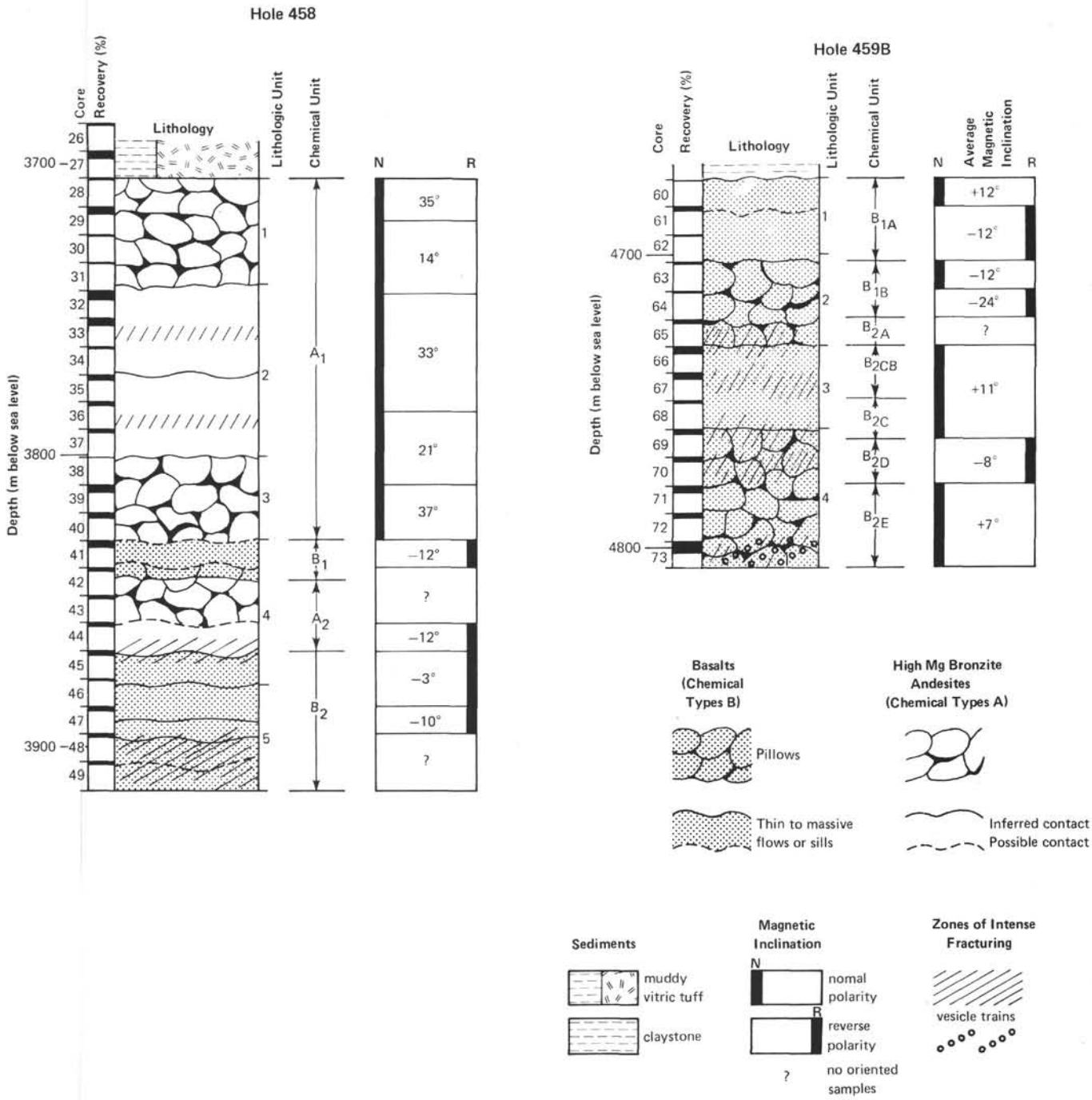

Figure 2. Basement lithologic, chemical, and magnetic stratigraphy, Sites 458 and 459.

the rock, where these isolated plagioclase spherulites first occur, they become so abundant that they coalesce and the entire zone of the pillow is highly vesicular. Meijer et al. (this volume) speculate that segregation of dissolved volatiles into vesicles locally reduced the water content of the glass, allowing plagioclase to crystallize. However, apart from the vesicles, these plagioclase spherulites occur in precisely the same position and have the same form as in weakly vesicular abyssal tholeiites (e.g., Kirkpatrick, 1978; Natland, 1978, 1980). This could mean that it was the crystallization of the plagioclase in the spherulites that forced the segregation of vesicles, not the other way around.

The clinopyroxene microlites in these rocks have terminations which generally spread out into two or more dendritic or skeletal arms, a feature typical of crystals that grew at high rates of cooling (Fig. 3E). Other, less abundant clinopyroxenes have several curved radiating

Table 1. Average of chemical types and subtypes of boninites and island arc tholeiites, DSDP Holes 458 and 459B.[a]

	Hole 458							Hole 459B						
	Ave. Type A_1 Boninite 1(21)[b]	Sample 458-29-2, 37 cm Boninite 2	Ave. of Bronzite Andesite Flow Cores 32-35 3(6)[b]	Sample 458-40-2, 90 cm Boninite 4	Type B_1 Basalt 5[b]	Ave. Type A_2 Boninite 6(6)[b]	Ave. Type B_2 Basalt 7(6)[b]	Ave. Type B_{1A} Basalt 8(3)[b]	Ave. Type B_{1B} Basalt 9(2)[b]	B_{2A} Basalt 10	Ave. Type B_{2B} Basalt 11(3)[b]	Ave. Type B_{2C} Basalt 12(2)[b]	Ave. Type B_{2D} Basalt 13(2)[b]	Ave. Type B_{2E} Basalt 14(4)[b]
SiO_2	55.0	52.0	58.5	52.8	53.2	53.9	52.0	54.3	51.2	52.6	56.7	57.7	55.7	55.1
TiO_2	0.32	0.36	0.31	0.35	1.13	0.52	1.10	0.69	0.83	1.21	0.97	0.74	0.91	1.13
Al_2O_3	15.2	14.4	14.2	14.9	15.5	14.3	14.0	14.6	14.3	13.9	13.1	13.3	14.3	13.9
$Fe_2O_3^T$	9.31	10.23	9.12	10.24	9.66	10.54	13.63	9.95	10.67	13.63	11.89	10.82	11.01	11.91
MnO	0.12	0.12	0.11	0.09	0.06	0.13	0.11	0.14	0.14	0.16	0.15	0.12	0.11	0.11
MgO	6.87	9.71	5.62	8.97	3.73	6.21	6.69	5.78	9.64	6.07	5.09	5.52	5.40	5.19
CaO	9.59	8.70	9.79	7.98	6.12	8.33	6.55	10.82	8.47	6.06	7.25	7.63	8.25	7.40
Na_2O	2.60	2.63	2.48	2.47	5.70	2.65	3.31	2.87	3.31	3.73	3.18	3.15	3.71	4.02
K_2O	0.98	0.88	0.96	1.03	1.52	0.66	0.75	0.48	0.62	0.89	0.98	1.29	0.91	1.02
P_2O_5	0.03	0.01	0.04	0.01	0.20	0.03	0.09	0.07	0.09	0.06	0.08	0.08	0.10	0.12
Total	100.02	99.01	101.13	98.86	96.82	97.27	98.23	99.70	99.27	98.35	99.39	100.35	100.40	99.90
Mg/Mg + Fe	0.594	0.653	0.550	0.634	0.433	0.558	0.493	0.535	0.641	0.462	0.459	0.502	0.493	0.463
Trace Elements (ppm)														
Ni	76	76	61	97	11	74	29	56	60	24	23	29	26	14
Cr	212	216	185	290	11	167	33	153	62	13	15	23	38	16
Sr	105	103	103	104	169	110	139	119	125	125	108	130	135	134
Zr	33	30	32	38	101	49	62	37	53	68	53	49	59	69
Y	3	2	8	6	31	15	24	15	29	27	23	19	26	32
Nb	2	3	5	7	7	4	5	4	6	6	2	3	4	5
CIPW Norms[c]														
Q	4.31	0.00	10.86	0.82	0.00	6.25	0.91	4.49	0.00	0.52	8.56	8.06	3.54	2.19
Or	5.78	5.19	5.67	6.08	8.97	3.90	4.43	2.83	3.66	5.25	5.78	7.61	5.37	6.02
Ab	21.98	22.24	20.97	20.88	44.24	22.41	27.99	24.27	27.99	31.54	26.89	26.63	31.37	33.99
An	26.90	24.87	24.77	26.51	12.21	25.16	21.12	25.52	22.32	18.55	18.57	18.33	19.67	16.86
Ne	0.00	0.00	0.00	0.00	2.15	0.00	0.00	0.00	0.00	0.00	0.00	0.00	0.00	0.00
Di Wo	8.54	7.59	9.81	5.42	7.02	6.65	4.49	11.54	7.96	4.63	7.03	7.92	8.59	7.95
Di En	4.83	4.65	5.21	3.24	3.19	3.49	2.22	6.09	4.89	2.22	3.29	3.96	4.26	3.77
Di Fs	3.34	2.51	4.29	1.90	3.77	2.96	2.18	5.10	2.61	2.35	3.66	3.78	4.15	4.07
Hy En	12.39	15.19	8.89	19.15	0.00	12.10	14.52	8.45	8.47	13.07	9.55	9.90	9.29	9.26
Hy Fs	8.58	8.19	7.32	11.22	0.00	10.26	14.22	7.07	4.52	13.86	10.62	9.45	9.06	9.99
Ol Fo	0.00	3.10	0.00	0.00	4.30	0.00	0.00	0.00	7.53	0.00	0.00	0.00	0.00	0.00
Ol Fa	0.00	1.84	0.00	0.00	5.61	0.00	0.00	0.00	4.44	0.00	0.00	0.00	0.00	0.00
Mt	1.72	1.90	1.69	1.90	1.79	1.95	2.53	1.84	1.98	2.53	2.20	2.01	2.04	2.20
Il	0.61	0.69	0.59	0.67	2.15	0.99	2.10	1.31	1.58	2.30	1.85	1.41	1.73	2.15
Ap	0.07	0.02	0.09	0.02	0.46	0.07	0.21	0.16	0.21	0.14	0.19	0.19	0.23	0.28

[a] Compiled from data of Wood et al. (this volume).
[b] Number of analyses in parentheses if more than one.
[c] Calculated assuming $Fe^{2+}/(Fe^{2+} + Fe^{3+}) = 0.86$.

Table 2. Summary of phenocryst and groundmass crystal morphologies in Hole 458 boninite pillows.

	→ Toward Pillow Interiors →					
Pillow Zones	1	2	3	4	5	6
groundmass	glass	augite spherulites + glass	skeletal augite microlites + isolated plagioclase spherulites	augite microlites + coalesced plagioclase spherulites	augite microlites + fan and bowtie plagioclase spherulites	augite microlites + plagioclase microlites
phenocrysts	?		euhedral bronzite (no dendrites) augite with dendrites blocky augite common bronzite-augite intergrowths (1) bowtie (2) bronzite with augite overgrowths		euhedral bronzite (some with dendrites) granular augite (rare dendrites) blocky augite rare rare bronzite-augite intergrowths, none with overgrowths	

axial projections (described as "coxcomb" morphology by Meijer et al., this volume) that are a form of spherulite. One of these is shown lower center in Figure 3E.

The most completely crystallized rocks of Lithologic Unit 1 contain clinopyroxene microlites in a matrix of fine but distinct needlelike plagioclase crystals, arranged in fans or sheafs. In Lithologic Unit 3, some intergranular rocks with abundant plagioclase are interbedded with the glassier clinopyroxene-rich rocks, but the degree of alteration makes it uncertain that these originally had closely similar compositions. No complete flows or pillows with textures ranging from spherulitic to intergranular were found among the Lithologic Unit 3 rocks.

The acicular clinopyroxenes and spherulitic plagioclases are the only minerals that appear to have formed during the final stages of pillow extrusion. All other minerals in the rocks are microphenocrysts that grew prior to pillow extrusion, forming distinctive dendritic projections along their major crystallographic axes (Fig. 4A). Orthopyroxenes, which have bronzite compositions, tend to be euhedral in glassy and spherulitic samples or complexly intergrown with augite. They have no dendritic or other overgrowths in quenched glassy samples but can have dendritic projections in samples cooled somewhat more slowly (Fig. 4B).

Microphenocrysts of both augite and bronzite in Lithologic Units 1 and 3 range from simple euhedral crystals to complexly intergrown multicrystal aggregates. The latter are less abundant in Lithologic Unit 3 than in Unit 1 and in the few thin sections prepared on board the *Glomar Challenger* are also altered, or partly altered, to clays. Only two thin sections were prepared on board ship from the boninite series lavas of Lithologic Unit 4 (Chemical Type A_2). These were intensely altered, had only rare microphenocrysts, and consisted primarily of clinopyroxene microlites surrounded by spherulitic fans of plagioclase. The remaining discus-

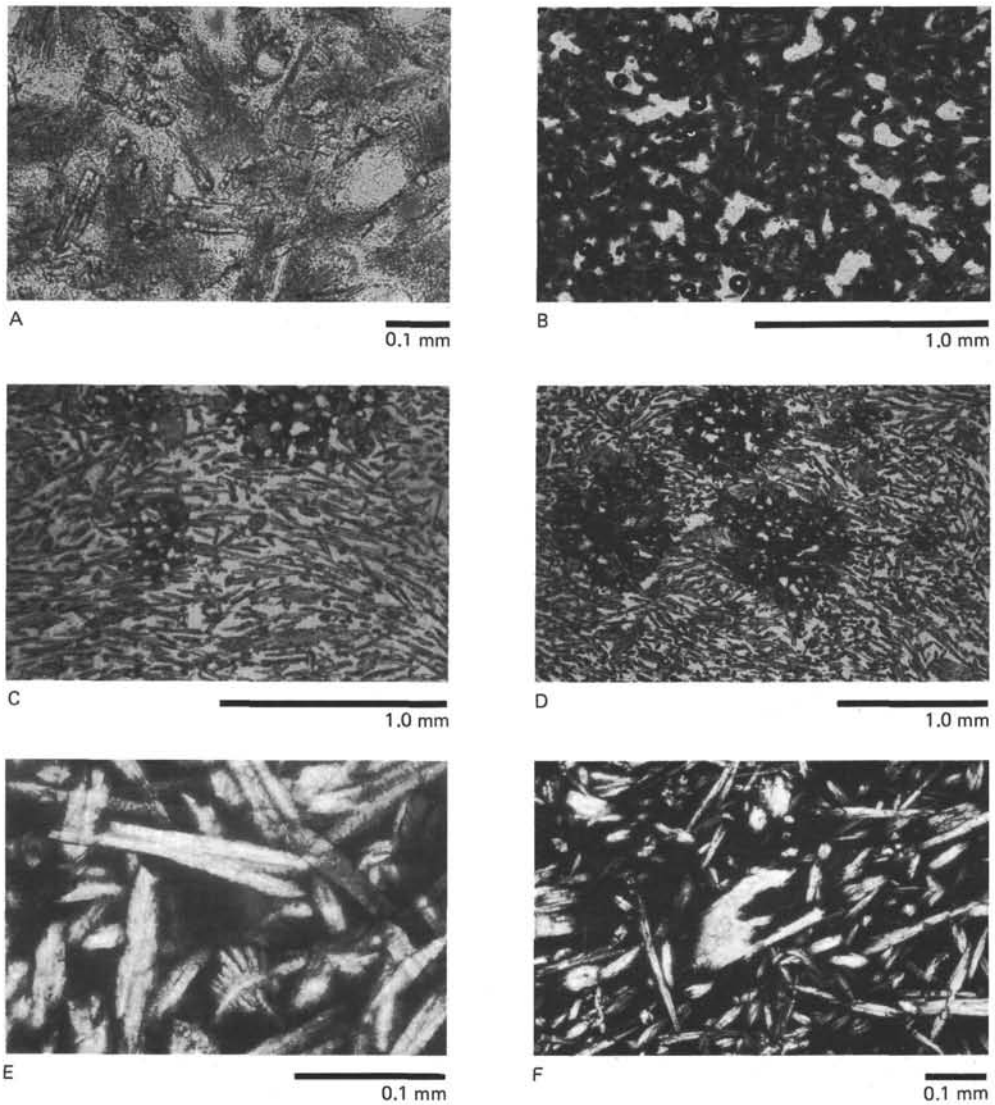

Figure 3. Crystal morphologies is glassy boninites, Hole 458. A. Sample 458-40-1, 33–35 cm. Plane light. Sperulitic clinopyroxene in altered glassy matrix of Lithologic Unit 3 boninite pillow rim. B. Sample 458-28-1, 64–67 cm. Plane light. Clinopyroxene microlites, many with fibrous sperulitic projections (dark) in glassy matrix (light), Lithologic Unit 1 boninite. C. Sample 458-28-1, 142–146 cm. Plane light. Clinopyroxene microlites in glassy Lithologic Unit 1 boninite pillow rim. Subparallel arrangement of microlites may have been the result of the glass having been stretched plastically during pillow formation. Three vesicular plagioclase spherulites are also shown. D. Sample same as C in plane light but at reduced magnification to show augite microphenocrysts and larger vesicular plagioclase spherulites. E. Sample 458-29-1, 1–3 cm. Crossed nichols. Detail of clinopyroxene microlites, showing development of central 001 grooves leading to bifurcation of the central crystal into two arms. A branched spherulite is at bottom. F. Sample 458-30-1, 101–104 cm. Crossed nichols. Center is an irregular augite microphenocryst with dendritic projections. At lower right are two intergrown clinopyroxene microlites.

sion of microphenocrysts therefore applies to Lithologic Unit 1 (Type A_1) only.

Clinopyroxene microphenocrysts can have irregular extinction and blocklike morphology (Fig. 4C) produced in part by what may have been a type of heterogeneous nucleation (attachment of crystals along other crystal faces, sometimes but not always in optical continuity). A typical growth feature is to have blocklike crystals attached to each other endwise, resulting in skeletal composite crystals (Fig. 4D). This type of growth is reminiscent of the growth of certain types of plagioclase microphenocrysts in abyssal tholeiites (compare to Natland, 1978, fig. 8, A and D).

Most bronzites occur as single crystals. The one in Figure 4E has a twinned termination (left side). The thin bright lines that show up when the rest of the crystal is at extinction appear to be clinopyroxene exsolution lamellae. Other bronzite crystals occur in bow tie intergrowths with clinopyroxene (Fig. 5, A and B). In glassy samples they are quite commonly irregular in shape with thin rims of clinopyroxene (Fig. 5C). Multicrystal intergrowths of bronzite and clinopyroxene show blocky

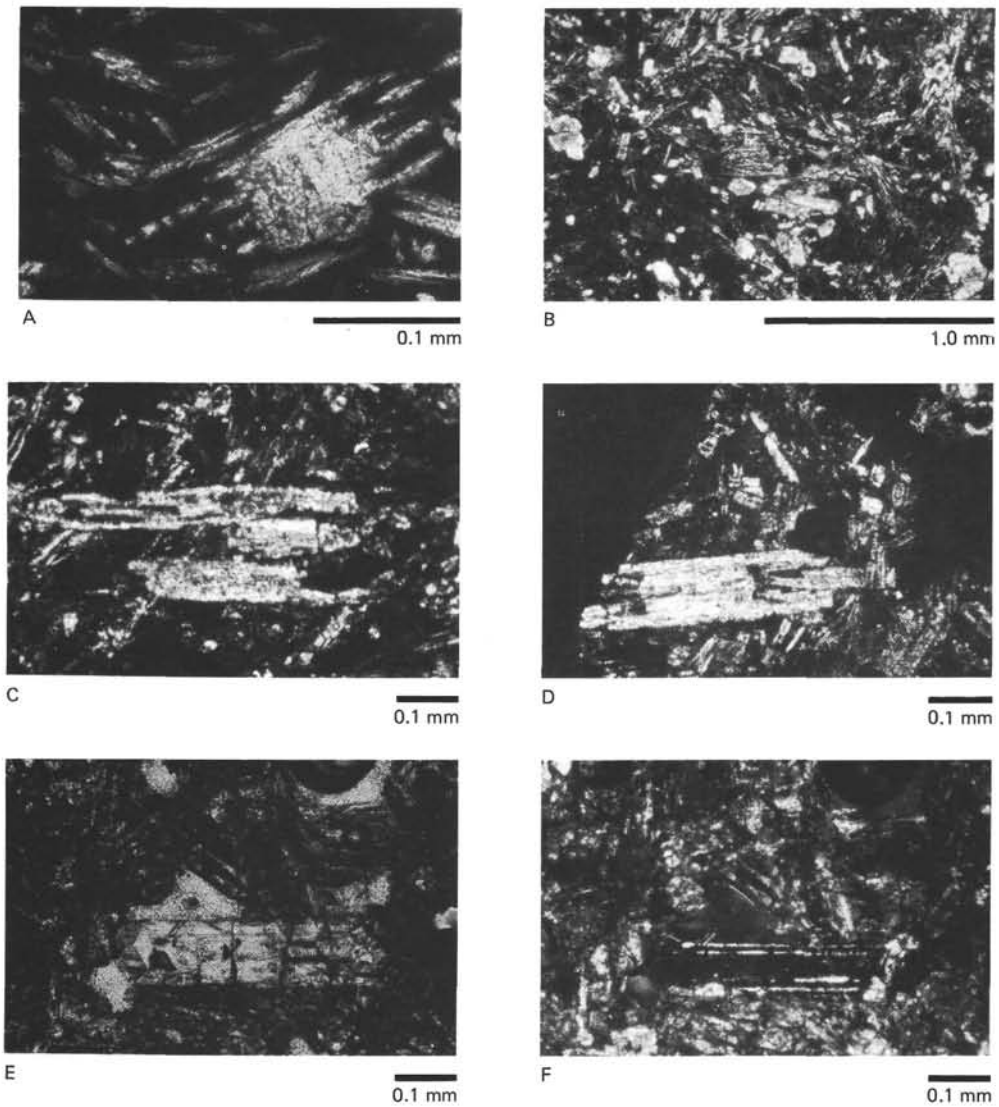

Figure 4. Pyroxene phenocrysts and spherulitic groundmass in Hole 458 boninites. A. Sample 458-29-1, 1–3 cm. Crossed nichols. Augite microphenocryst with dendritic spines growing from both ends. B. Sample 458-28-1, 9–13 cm. Crossed nichols. Typical fine fibrous spherulitic plagioclase growing between clinopyroxene microlites in one of the more crystalline boninites of Lithologic Unit 1. C. Sample 458-30-1, 71–73 cm. Crossed nichols. "Blocky" augite microphenocryst in Lithologic Unit 1 boninite. Growth was by lateral attachment, causing parallel crystals, but upper-left crystal appears to have grown partly by filling in of space between dendritic spines, such as those of Figure 4A. D. Sample 458-30-1, 71–73 cm. Crossed nichols. Another blocky augite glomerocryst. Blocky additions at right end have trapped groundmass material within the glomerocryst. E. Sample 458-28-1, 64–67 cm. Plane light. Bronzite microphenocryst. Note "serrated" crystal termination on left side of crystal. F. Same sample as E but with nichols crossed. Thin clinopyroxene lamellae extend the length of the crystal up to the "serrated" crystal termination at the left end, where they stop.

growth morphology (Fig. 5, D and E), but in some of them blocky growth has given way (at the crystal extremities) to development of thin dendritic clinopyroxene arms enclosing bronzite along 001 crystal faces (Fig. 6, A and B). Pyroxene compositional variations in this type of growth will be discussed later.

Finally, some clinopyroxene phenocrysts have extremely irregular zoning (Fig. 6, C and D). This pattern of growth appears to be a combination of blocky growth and dendritic extension, perhaps reflecting a range of undercoolings.

In summary, the sequence of mineral crystallization in these rocks is (1) bronzite, (2) clinopyroxene, (3) plagioclase, and (4) Fe–Ti oxides. Olivine and clinoenstatite do not occur, nor do Fe–Ti oxides in glassy samples. Scattered Fe–Ti oxides occur, however, in the coarser-grained rocks of Lithologic Units 2 and 3. Meijer et al. (this volume) report that chrome spinel occurs as rare tiny crystals surrounded by augite microphenocrysts.

Table 2 summarizes crystal morphologies in Lithologic Unit 1 boninite series lavas. The six divisions of crystal morphologies shown are inferred to represent

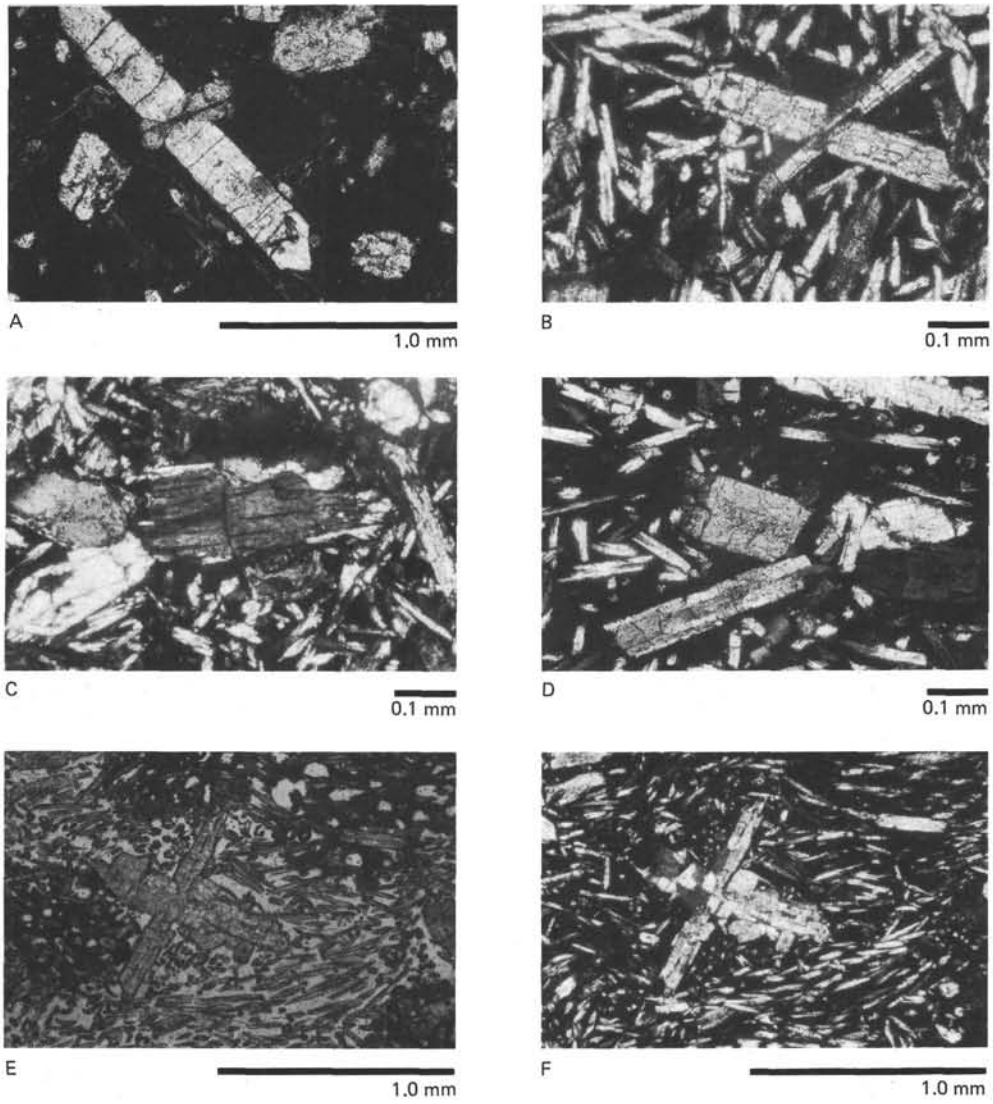

Figure 5. Two-pyroxene intergrowths in Hole 458 boninites. A. Sample 458-28-1, 9–13 cm. Crossed nichols. Bow tie intergrowth of bronzite (longer crystal) and twinned augite. Note spherulitic plagioclase in matrix. B. Sample 458-28-1, 142–146 cm. Crossed nichols. Intergrowth of bronzite (wide crystal) and elongate augite, in hyalopilitic matrix with no plagioclase. Crystals are smaller than in 5A and have less regular terminations. C. Sample 458-29-1, 1–3 cm. Crossed nichols. Irregular-shaped bronzite rimmed with augite. Note dendritic projections on skeletal bronzite, lower left. D. Sample 458-28-1, 142–146 cm. Crossed nichols. Intergrown clinopyroxene microphenocrysts with typical separations into two dendritic "arms." Microphenocryst at lower left has a bronzite core (darker gray at this orientation relative to extinction) marginally "zoned" with narrow clinopyroxene borders which project into the glass beyond the bronzite. E. Sample 458-28-1, 142–146 cm. Plane light. Complexly intergrown pyroxene microphenocrysts in a hyalopilitic matrix. F. Sample 458-28-1, 142–146 cm. Same as 5E, except that nichols are crossed. The "blocky" growth pattern of the larger augitic portion of the intergrowth is revealed. The two more slender arms also contain intergrown bronzite, shown in Figure 6A.

progressive distance from pillow rims to pillow interiors, hence decreasing undercooling, of rocks that are essentially identical chemically. The zones correspond approximately with the pillow zones of Kirkpatrick (1978). The ranges in chemistry within Lithologic Units 1 and 3 probably would not affect these relations other than perhaps to modify abundances of microphenocrysts. For example, it is probably that the more magnesian *fresh* lavas of Chemical Type A_1 in Core 29 (Fig. 2) have more bronzite phenocrysts than other lavas of this general chemical type. Table 2 illustrates that apart from increasing crystallinity of the groundmass and abundance of groundmass plagioclase, decreased undercooling modifies microphenocryst relationships considerably. The abundance of intergrowths is diminished, and there is a clear tendency for individual phenocrysts rather than clumps to form. Dendritic overgrowths do not occur on clinopyroxene but can on bronzite. These relationships favor the interpretation that the microphenocrysts themselves grew at conditions of heightened undercooling rather than near equilibrium in a slowly cooled magma chamber. Probably they formed

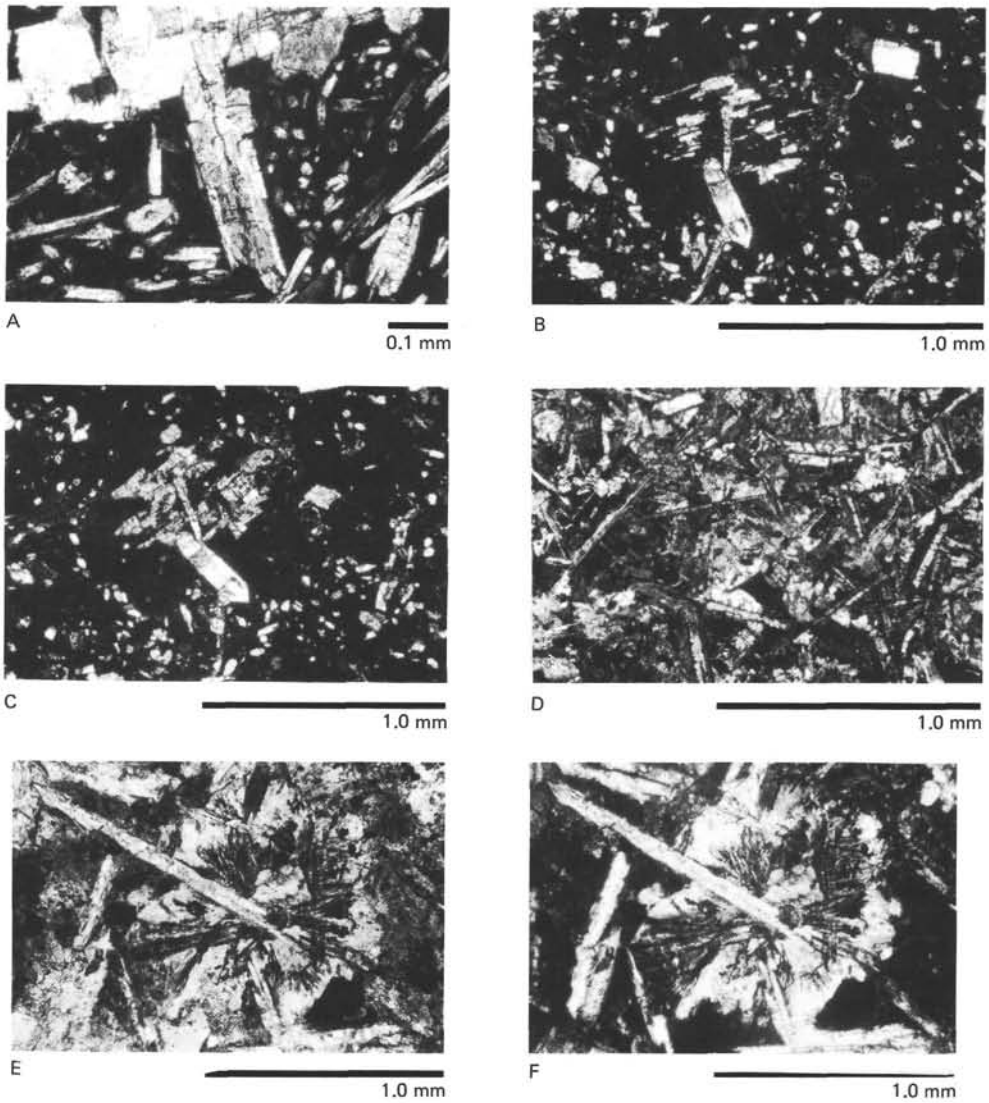

Figure 6. Two-pyroxene intergrowths in glassy boninites and groundmass textures in massive bronzite andesites. A. Sample 458-28-1, 142–146 cm. Crossed nichols. Detail of the lower arm of the intergrowth shown in Figure 5, E and F. Outer portions of "arm" (augite) appear to combine a "blocky" growth morphology (nearer the intersection with the larger cross-arm) and separation into two quasi-dendritic branches, separated by bronzite. B and C. Sample 458-28-1, 9–13 cm. Crossed nichols. Two views of a single complexly intergrown glomerocryst of augite and bronzite, at slightly different angles. The extinct interior of the glomerocryst in B is bronzite, the rest augite. Turning the stage to C puts other augitic portions of the glomerocryst into extinction but brings bronzite and some augite out of extinction. D. Sample 458-33-1, 9–13 cm. Crossed nichols. Subophitic bronzite andesite with elongate euhedra of augite and some of plagioclase in a matrix consisting mainly of irregular anhedral plagioclase. E and F. Sample 458-31-1, 2–7 cm. In plane light and with nichols crossed, respectively. Spherulitic interstitial plagioclase surrounding plagioclase euhedra in groundmass of bronzite andesite. The radiating pattern is accentuated by inclusions of a needlelike mineral (quartz?) with higher relief.

as the lavas were extruded and continued to grow as they flowed, prior to budding of pillows. It is also probable, therefore, the composition of the fresh lavas is close to that of the liquid—without accumulations of phenocrysts.

The coarse-grained massive flows of Lithologic Unit 2 share some of the petrographic features of the pillows. Primarily, the crystallization sequence is the same—bronzite, clinopyroxene, plagioclase, and Fe-Ti oxides. However, apart from euhedral orthopyroxenes, it is difficult to identify phenocrysts that are discernibly larger than the augites and feldspars surrounding them. These massive rocks, however, have a more fractionated composition than most of the pillows (Table 1), hence their crystallization cannot strictly be linked to the sequence of decreasing undercooling of Table 2. One important feature of these massive flows is that they evidently underwent localized *in situ* magmatic differentiation. The principal evidence for this is the occurrence of coarse patches of spherulitic plagioclase enclosing more calcic euhedral plagioclase laths (Fig. 6, E and F). The laths themselves have spherulitic terminations, and the

patchy feldspar surrounding them is intergrown with a clear mineral that may be quartz, arrayed in a crudely radial pattern in Figure 6, E and F. In some coarse-grained samples, there are fairly large crystals of free quartz, irregular in shape, associated with similar patchy feldspar, and opaque minerals. This is in accord with the high SiO_2 (58–59%) and normative quartz (8–10%) of the massive rocks (Table 1).

MINERALOGY OF THE HOLE 458 BONINITE SERIES LAVAS

To elucidate the effects of rapid cooling on the boninite series pillow lavas of Hole 458, electron microprobe analyses of orthopyroxenes and clinopyroxenes were obtained from a glassy sample having particularly prominent two-pyroxene intergrowths. The data were obtained on an ARL 9-channel electron microprobe at the Smithsonian Institution and are listed in Table 3.

In all cases, the orthopyroxenes are bronzites[2] and the clinopyroxenes augites. The normalized pyroxene end-members, calculated from structural formulae in Table 3, are plotted on a pyroxene quadrilateral (Fig. 7A). Several distinctions are made among the plotted augites according to their occurrence as individual crystals (microphenocrysts or microlites) or as parts of two-pyroxene intergrowths. It is readily apparent that most of the bronzites are very nearly identical in composition, regardless of their occurrence as individual crystals or in crystal aggregates. The two analyses that fall outside the grouping have somewhat higher structural Wo and Fs, which may reflect partial involvement of the probe beam with clinopyroxene and glass, respectively.

In contrast, there is a clear compositional difference between augite crystals, and augite borders on bronzite, the latter being both more calcic and iron-rich. The borders are also richer in tetrahedrally coordinated aluminum (Al_Z) and Ti, as shown on Figure 8.

I interpret these data to mean that the augite borders owe their compositions to growth from glass enriched in Ca, Fe, Al, and Ti caused by the prior growth of the bronzite cores. This could have been a disequilibrium effect caused by reduced diffusion rates of polymers containing these elements in the glass occasioned by heightened undercooling and increased melt viscosity during pillow extrusion. Probably the growth of the crystals and their borders was nearly simultaneous. In some cases, the augite borders extend somewhat beyond the ends of the bronzite cores (Figs. 4D and 5A), a morphology comparable to the dendritic projections on augite microphenocrysts (Fig. 4A).

For comparison, the data of Sharaskin (this volume) and Meijer et al. (this volume) are plotted on Figure 7B. Their samples include several from the massive flows of Lithologic Unit 2 (Cores 31 and 33). Augites reported by Sharaskin (this volume) from these intervals form subophitic intergrowths with plagioclase and are normally zoned. The sense of that zoning, as indicated on Figure 7B, is toward *less* calcic, more iron-enriched compositions than the augite borders on bronzites of Figure 7A. This is presumably a consequence of reaction with successively fractionated interstitial melt compositions during *in situ* magmatic differentiation. The orthopyroxenes reported by Sharaskin (this volume) and Meijer et al. (this volume) are also bronzites, very similar to those of Table 3, although in both reports they were from samples of Chemical Type A_2 (Lithologic Unit 4).

The type of crystal intergrowth discussed here has been noticed previously in boninites from other localities. Dallwitz et al. (1966) described it as "marginal zoning" in samples from Cape Vogel, and presented microprobe data for augite mantling clinoenstatite. Cameron et al. (1979) figured a boninite from the Troodos ophiolite, with augite microlites identical to those described here, and an orthopyroxene microphenocryst "jacketed" by augite. This type of crystal intergrowth therefore seems to be a characteristic feature of glassy boninitic lavas. On the basis of the data presented here, augite borders on Mg–Fe pyroxene evidently occur because of changes in the properties of melts near growing Mg–Fe pyroxenes at the marked undercoolings sustained by the margins of extruding pillows.

Other types of marginal zoning have been described for more mafic boninites, including rims of clinoenstatite on olivine, bronzite on olivine, bronzite on clinoenstatite (Komatsu,1980), clinoenstatite on bronzite, and augite on clinoenstatite (Dallwitz et al., 1966; Kuroda et al., 1978; Komatsu, 1980). Some of these, such as feathery terminations of clinopyroxene on clinoenstatite microlites described by Dallwitz et al. (1966), clearly also originated in response to high undercooling. Komatsu (1980), however, inferred a reaction relationship between clinoenstatite and olivine. In some of the samples he examined and in samples described by Kuroda et al. (1978), the bordering compositions are *more* magnesian than the core minerals (i.e., clinoenstatite rims on bronzite). Komatsu suggested this effect was caused by an increase of magma temperatures upon extrusion because of an oxidation reaction (e.g., Smith, 1969). Clearly, pyroxene interrelationships in boninites are complex. The data and arguments presented here point to the importance of kinetic factors during rapid cooling as the cause for at least some of these features.

Bougault et al. (this volume) presented microprobe data for pyroxenes in a remarkable specimen from Core 44, Section 1 (Chemical Type A_2), plotted here as Figure 7C. In this specimen, there is a wider range of both ortho- and clinopyroxene compositions, including the occurrence of strikingly iron-enriched ferroaugite and ferrohedenbergite phenocrysts. Bronzite phenocrysts are similar to those of Table 3, but orthopyroxene microlites are more calcic, with some either forming rims on, or being rimmed by, iron-rich clinopyroxene.

These iron-rich clinopyroxene phenocrysts may be unique among lavas. They are known elsewhere only from granophyric members of ferrogabbros (i.e., the Skaergaard intrusion; Wager and Brown, 1967) and in quartz syenites, alkali granites, and shonkinites, where they are commonly associated with fayalite (Deer et al.,

[2] The bronzites have more than 5% Wo in their structural formulae, hence they resemble magnesian pigeonites. However, they are too magnesian, strictly speaking, to be so classified, so I refer to them here as bronzites (see Fig. 7C).

Table 3. Electron microprobe analyses of pyroxenes in boninite Sample 458-28-1, 142–146 cm.

	Orthopyroxenes											
	Analysis Number[a]											
	49	54	55	57	62	63	66	67	68	69	72	73
SiO_2	49.07	53.38	54.46	52.66	54.89	54.22	54.62	54.81	53.99	54.98	54.54	54.60
Al_2O_3	8.48	1.69	1.54	2.93	1.19	2.94	1.71	1.60	2.51	1.59	1.57	2.94
FeO*	16.78	8.98	9.04	10.06	9.80	9.46	10.64	10.87	10.78	10.99	10.88	10.00
MgO	22.11	27.52	29.16	28.78	30.02	29.66	28.93	29.31	29.11	29.14	28.99	29.12
CaO	3.37	6.14	3.24	3.22	2.67	2.97	2.96	2.69	2.66	2.84	2.80	2.70
Na_2O	0.13	0.07	0.05	0.10	0.05	0.05	0.05	0.05	0.05	0.05	0.05	0.05
K_2O	0.05	0.01	0.01	0.01	0.01	0.01	0.01	0.01	0.01	0.01	0.01	0.01
TiO_2	0.21	0.09	0.04	0.16	0.07	0.10	0.09	0.08	0.13	0.08	0.05	0.08
	100.20	97.88	97.91	97.91	98.64	99.25	98.95	99.36	99.18	99.62	98.83	99.44
	Structural Formulae Computed on the Basis of 6(O)											
Si	1.793 } 2.00	1.940 } 2.00	1.965 } 2.00	1.908 } 2.00	1.962 } 2.000	1.963 } 2.000	1.955 } 2.000	1.954 } 2.000	1.929 } 2.000	1.956 } 2.000	1.956 } 2.000	1.936 } 2.000
Al	0.207	0.060	0.035	0.092	0.038	0.077	0.045	0.046	0.071	0.044	0.044	0.64
Al	0.154	0.012	0.031	0.033	0.012	0.046	0.027	0.021	0.035	0.023	0.022	0.059
Fe	0.513	0.273	0.273	0.305	0.293	0.281	0.319	0.324	0.322	0.327	0.326	0.297
Mg	1.204	1.491	1.569	1.554	1.600	1.568	1.543	1.558	1.550	1.546	1.550	1.539
Ca	0.132 } 2.024	0.239 } 2.024	0.125 } 2.004	0.125 } 2.029	0.102 } 2.014	0.113 } 2.015	0.114 } 2.010	0.103 } 2.012	0.102 } 2.018	0.108 } 2.011	0.108 } 2.012	0.103 } 2.004
Na	0.009	0.005	0.004	0.007	0.004	0.003	0.004	0.004	0.004	0.004	0.004	0.003
K	0.002	0.001	0.001	0.001	0.001	0.001	0.001	0.001	0.001	0.001	0.001	0.001
Ti	0.006	0.003	0.001	0.004	0.002	0.003	0.002	0.002	0.004	0.002	0.001	0.002
	$Wo_{7.1}En_{65.1}Fs_{27.7}$	$Wo_{11.9}En_{74.4}Fs_{13.6}$	$Wo_{6.4}En_{79.8}Fs_{13.9}$	$Wo_{6.3}En_{78.3}Fs_{15.4}$	$Wo_{5.1}En_{80.2}Fs_{14.7}$	$Wo_{5.6}En_{78.3}Fs_{15.4}$	$Wo_{5.8}En_{78.1}Fs_{16.1}$	$Wo_{5.2}En_{78.5}Fs_{16.3}$	$Wo_{5.2}En_{78.5}Fs_{16.3}$	$Wo_{5.5}En_{78.0}Fs_{16.5}$	$Wo_{5.5}En_{78.1}Fs_{16.5}$	$Wo_{5.3}En_{79.4}Fs_{15.3}$

[a] Orthopyroxenes are microphenocrysts or parts of two-pyroxene intergrowths. 49 and 54 may show effects of partial overlap of the probe beam with glass and clinopyroxene, respectively.
[b] Clinopyroxene Analyses 50, 58, 70, 71, and 74 are of rims of bronzite. All others are cores to larger microphrenocrysts or grains in two-pyroxene intergrowths.

Table 3. (Continued).

	Clinopyroxenes										
	Analysis Number[b]										
47	50	52	53	56	58	59	61	70	71	74	
53.87	49.80	52.21	53.00	52.21	50.29	52.98	53.46	46.82	48.31	48.20	
2.33	7.53	2.66	2.00	2.19	5.60	2.10	2.18	9.49	7.63	6.12	
6.95	6.46	7.84	7.64	6.79	9.36	6.68	6.89	12.59	11.98	10.31	
19.45	16.12	17.61	20.15	18.79	15.86	19.32	19.23	11.21	13.43	15.03	
17.42	15.31	18.04	15.12	17.70	17.96	17.87	17.47	18.49	17.98	18.37	
0.05	1.47	0.14	0.14	0.15	0.16	0.11	0.15	0.17	0.22	0.29	
0.01	0.07	0.00	0.02	0.04	0.01	0.01	0.08	0.04	0.01	0.02	
0.37	0.76	0.14	0.09	0.10	0.34	0.11	0.10	0.55	0.38	0.31	
100.45	97.52	98.64	98.18	97.97	102.05	99.18	99.56	99.36	99.94	98.65	
Structural Formulae Computed on the Basis of 6(O)											
1.948 } 2.000	1.852 } 2.000	1.938 } 2.000	1.958 } 2.000	1.942 } 2.000	1.864 } 2.000	1.944 } 2.000	1.953 } 2.000	1.772 } 2.000	1.809 } 2.000	1.822 } 2.000	
0.052	0.148	0.062	0.042	0.058	0.136	0.056	0.047	0.228	0.191	0.178	
0.047	0.182	0.054	0.045	0.038	0.109	0.035	0.046	0.196	0.146	0.095	
0.210	0.201	0.244	0.236	0.211	0.290	0.205	0.211	0:399	0.375	0.326	
1.048	0.893	0.975	1.109	1.042	0.876	1.057	1.047	0.633	0.750	0.847	
0.675 } 1.995	0.610 } 2.016	0.718 } 2.006	0.599 } 2.003	0.706 } 2.013	0.713 } 2.011	0.703 } 2.009	0.684 } 2.006	0.750 } 2.009	0.722 } 2.021	0.744 } 2.043	
0.004	0.106	0.010	0.010	0.011	0.012	0.008	0.011	0.013	0.016	0.021	
0.001	0.003	0.000	0.001	0.002	0.001	0.001	0.004	0.002	0.001	0.001	
0.010	0.021	0.005	0.003	0.003	0.010	0.003	0.003	0.016	0.011	0.009	
$Wo_{34.9}En_{54.2}Fs_{10.9}$	$Wo_{35.8}En_{52.4}Fs_{11.8}$	$Wo_{37.1}En_{51.3}Fs_{12.6}$	$Wo_{30.8}En_{57.1}Fs_{12.1}$	$Wo_{36.0}En_{53.2}Fs_{10.8}$	$Wo_{38.0}En_{46.6}Fs_{15.4}$	$Wo_{35.8}En_{53.8}Fs_{10.4}$	$Wo_{35.2}En_{53.9}Fs_{10.8}$	$Wo_{42.1}En_{35.5}Fs_{22.4}$	$Wo_{39.1}En_{40.6}Fs_{20.3}$	$Wo_{38.8}En_{44.2}Fs_{17.0}$	

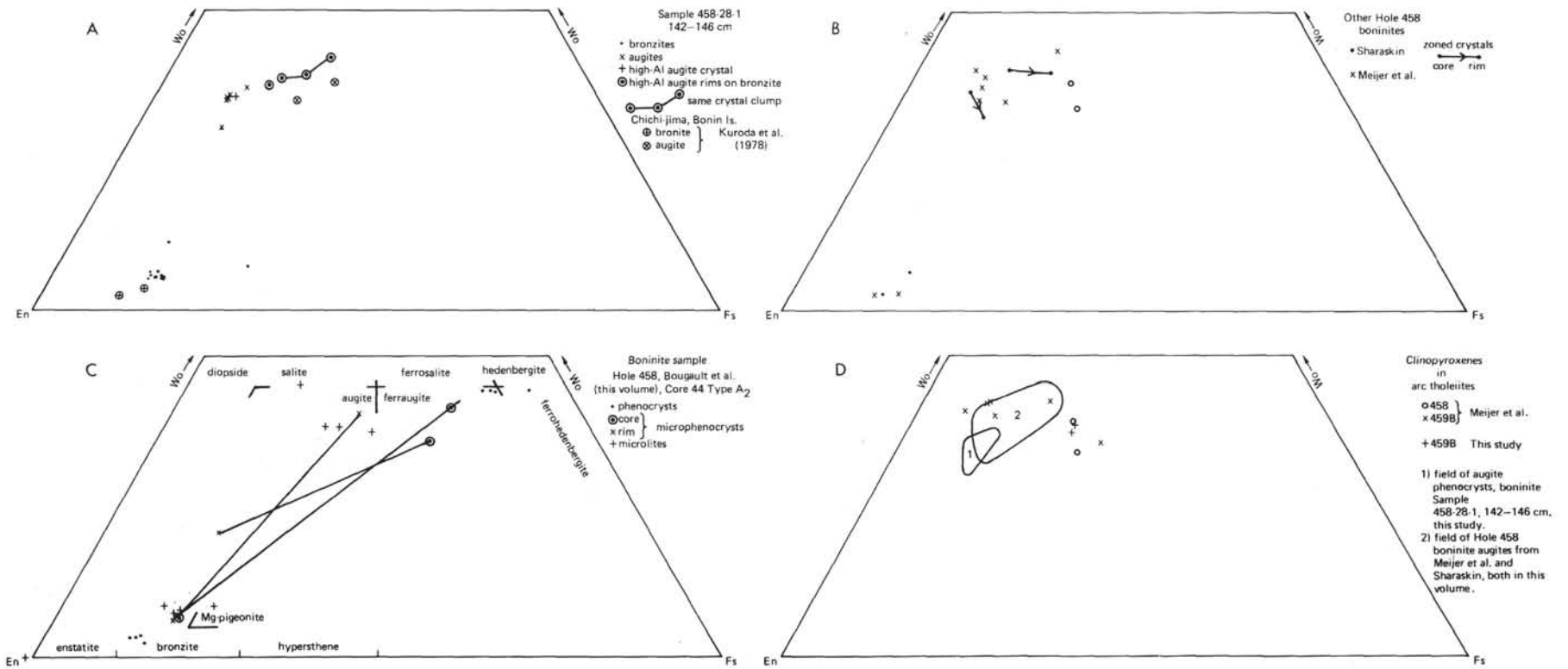

Figure 7. Pyroxene quadrilaterals comparing compositions of bronzites and augites in Sample 458-28-1, 142–146 cm (A), with pyroxenes reported in Meijer et al. (this volume) and Sharaskin (this volume) (B), and in Bougault et al. (this volume) (C). Also plotted on A are pyroxenes from boninites of Chichi-jima, Bonin Islands (Kuroda et al., 1978). Compositional boundaries for calcic pyroxenes are shown on C. D is augites from tholeiitic basalts, both this study and Meijer et al. (this volume). Fields on D are those of augites from A (field 1) and B (field 2).

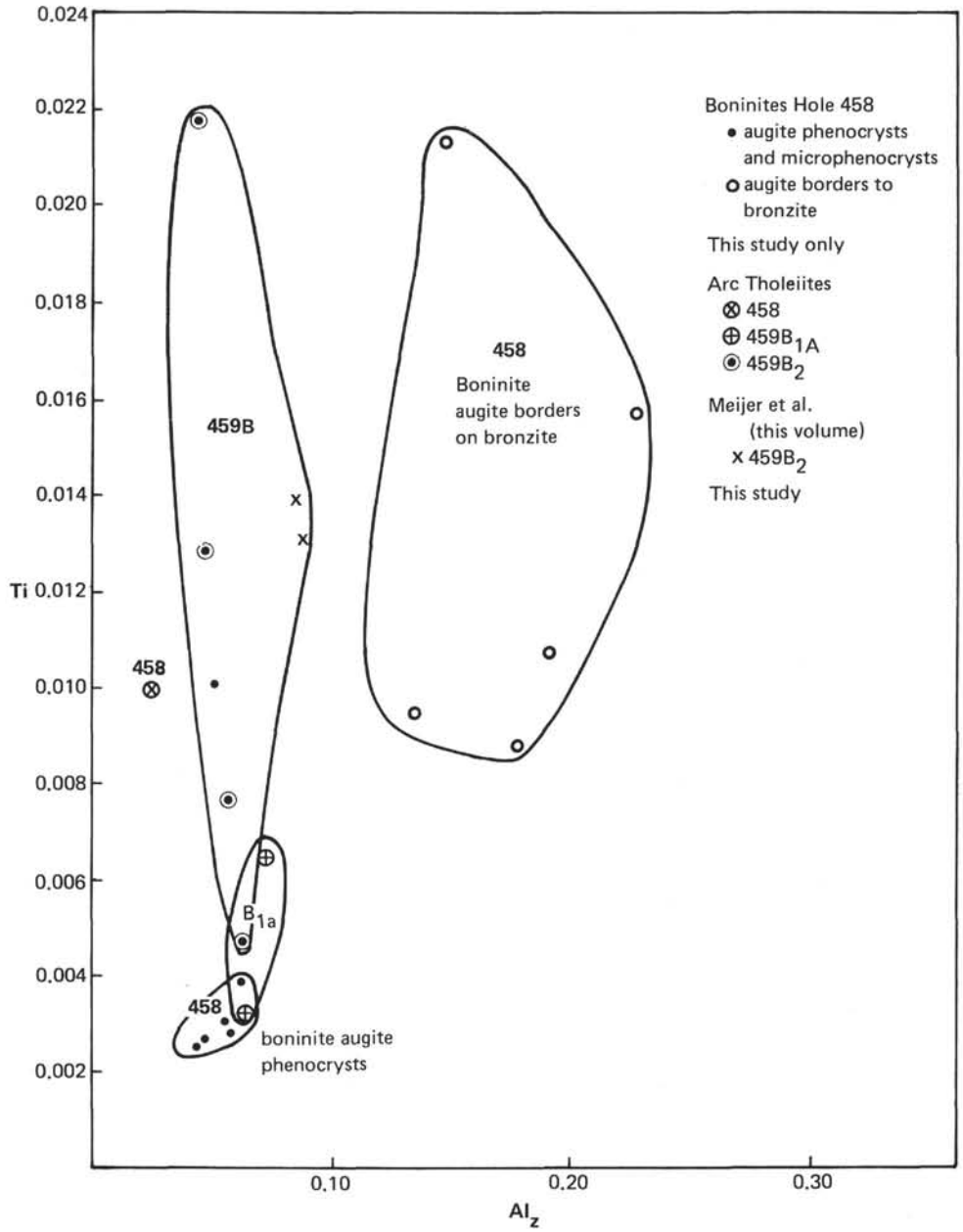

Figure 8. Ti versus Al_Z from pyroxene structural formulae. Data are from Tables 3 and 5, Meijer et al. (this volume) and Sharaskin (this volume).

1963, p. 68). They do not occur in calc-alkalic or tholeiitic lava suites of Japan (Kuno, 1968) or the Bonin and Mariana islands (Shiraki et al., 1978). The occurrences in coarse-grained rocks are generally thought to reflect circumstances of very low oxygen fugacity (Osborne, 1959, 1962, 1979). Such conditions would not be expected in magmas as hydrous as boninites generally seem to be. Dowty et al. (1974) report similar iron-rich clinopyroxenes in lunar pyroxene-phyric basalts, but they are not phenocrysts and, since they occur in the groundmass with metallic iron, they clearly formed at low oxygen fugacities.

Glass compositions in the sample analyzed by Bougault et al. (column A of Table 4) compare generally to glass compositions obtained in other samples from Hole 458 (columns B–D), including glass from Sample 458-28-1, 142–146 cm, for which pyroxene analyses are given in Table 3. All of these glasses have andesitic compositions comparable to a boninite series hypersthene andesite from the Bonin Islands (column F) reported by Kuroda et al. (1978). The pyroxene mineral relationships of Figure 7C differ so greatly from those shown in A and B that some unusual process has obviously occurred. With no data other than the mineral compositions for evidence, it would seem that magma hybridization between boninite and an iron-rich tholeiite granophyre has occurred, with incomplete mixing of two melt compositions providing two sharply contrasting domains of pyroxene crystallization within the same rock. If this interpretation is correct, it is also evidence for the

Table 4. Electron microprobe analyses of glasses in boninite pillow fragments, DSDP Hole 458, compared with silicic glass and lavas from the Bonin Islands.

	A	B	C	D	E	F	G
SiO_2	62.15	56.87	58.64	61.72	59.34	62.73	65.79
Al_2O_3	17.59	13.86	15.38	18.86	16.63	14.99	12.54
FeO*	5.45	7.67	8.02	4.26	6.19	6.49	5.62
MgO	1.56	6.62	4.56	0.64	1.50	1.69	1.56
CaO	6.72	9.80	8.74	5.24	6.34	5.99	4.54
Na_2O	1.07[a]	1.80	1.84	2.53	3.60	2.39	3.09
K_2O	0.49	0.40	0.35	0.56	0.56	0.89	0.90
TiO_2	0.26	0.29	0.52	0.33	0.08	0.26	0.31
P_2O_5	0.05	—	0.17	0.11	—	0.02	0.04
	95.34	97.31	98.34	94.26	94.33	95.45	94.39
Mg/Mg + Fe	0.338	0.606	0.503	0.211	0.302	0.317	0.331
	CIPW Norms[b]						
Q	33.94	13.36	18.58	30.32	17.13	26.34	29.82
C	3.20	0.00	0.00	4.83	0.00	0.00	0.00
Or	2.89	2.36	2.07	3.31	3.31	5.25	5.31
Ab	9.05	15.22	15.56	21.39	30.44	20.21	26.13
An	32.99	28.54	32.65	25.26	27.55	27.53	17.68
Di Wo	0.00	8.36	3.99	0.00	1.62	0.85	1.91
Di En	0.00	4.80	1.98	0.00	0.49	0.28	0.65
Di Fs	0.00	3.19	1.93	0.00	1.20	0.60	1.31
Hy En	3.87	0.00	0.00	1.59	3.23	3.92	3.22
Hy Fs	7.65	0.00	0.00	5.79	7.87	8.61	6.52
Mt	1.13	1.58	1.65	0.88	1.27	1.33	1.16
Il	0.50	0.55	0.99	0.63	0.15	0.50	0.59
Ap	0.12	0.00	0.39	0.25	0.00	0.05	0.09

Note: A, Sample 458-28-1, 142–146 cm, glass. B, Sample 458-39-1, 23–26 cm, glass (Meijer et al., this volume). C, Sample 458-43-2, 34–37 cm, glass (Meijer et al., this volume). D, Sample 458-44-1, 53–56 cm, glass (Bougault et al., this volume). E, Glass in boninite pillow, Tsuri-hama, Chichi-jima, Bonin Islands (Kuroda et al., 1980). F, Hypersthene andesite, near Omura Pier, Chichi-jima, Bonin Islands (Kuroda et al., 1980). G, Perlitic dacite, SE of Miyano-hama, Chichi-jima, Bonin Islands (Kuroda et al., 1978).

[a] Low Na_2O result of volatilization. New analysis by J. W. Hawkins has $Na_2O = 2.29\%$.

[b] Computed assuming $Fe^{2+}/Fe^{2+} + Fe^{3+} = 0.86$.

simultaneous availability of boninite and arc tholeiite magmas in the fore-arc region.

GEOTHERMOMETRY OF BONINITES

Because the phase relationships of coexisting orthopyroxenes and clinopyroxenes are reasonably well known, it is possible to estimate the temperature of crystallization of these minerals if both occur in the same rock. Here, the equation of Wood and Banno (1973) is used, as modified by Ishii (1980). The alternative modification of the Wood–Banno equation proposed by Wells (1977) produces almost identical results, to within a few degrees.

In a quenched pillow margin, because of rapid cooling rate, one might expect significant departures from equilibrium crystallization and hence in mineral compositions. We have seen, for example, that the compositions of augites in two-pyroxene intergrowths in a glassy sample are affected by the prior growth of bronzite. Such effects would make estimates of crystallization temperatures unreliable, based on mineral compositions. In this particular sample, choice of the wrong augite could result in temperature estimates low by over 100°C. A glassy rock may also have crystallized through a particular temperature range forming phenocrysts before quenching, which would produce a range of mineral compositions accurately reflected in a calculated range in the temperatures of crystallization. Here, to avoid the effects of kinetics of crystal growth, augite borders on bronzites have been excluded from the calculations. Also excluded are any grains which, on the basis of probe analyses, seem spuriously contaminated with glass or another mineral phase. The remaining mineral analyses are of larger microphenocrysts which are presumed to approximate crystallization nearer to equilibrium conditions. Ranges of compositions within these remaining augites and bronzites are assumed to reflect the combined effects of analytical precision and small degrees of crystallization fractionation.

Using the ratio Mg/Mg + Fe computed from the structural formulae of Table 3 as an index of fractionation, calculations were made for bronzite–augite pairs having both the highest and lowest values of this ratio among the analyzed pyroxenes (analysis pairs 55–53 and 69–52, respectively, of Table 3). These give temperatures of 1319°C and 1198°C, representing the possible maximum range of crystallization temperatures for the phenocrysts analyzed in the sample. Using the average bronzite and augite compositions gives a temperature of 1251°C.

One can compare these estimates of crystallization temperature with those of Ishii (1980) from lavas drilled during Leg 59 on the Palau-Kyushu Ridge (Site 448) and the West Mariana Ridge (Site 451), both older, rifted fragments of the Mariana arc. Ishii (1980) based his estimates on a variety of pyroxene geothermometers. On a plot of the ratio Mg/Mg + Fe in orthopyroxenes (X_{Fe}) versus crystallization temperature (Fig. 9), Ishii showed that clear differences exist in calculated temperatures of crystallization of pyroxenes in lavas of the two sites, with samples from the Palau-Kyushu Ridge having higher temperatures. He described the samples from Site 448 as "high-temperature tholeiites" and those from Site 451 as "low-temperature tholeiites" (two samples) and a calc-alkalic andesite (lowest temperature sample plotted on Fig. 9). It is evident from the figure that the boninite sample from Site 458 has much higher temperatures of crystallization than either tholeiitic basalts or calc-alkalic andesites from other portions of the Mariana arc, or Recent Japanese lavas from Hakone volcano. Temperatures of crystallization estimated from pyroxene compositions of other boninite-type lavas are also high. Based on data in Sharaskin et al. (1980), the temperature of crystallization of pyroxenes in a "marianite" sample dredged from the Mariana trench is 1128°C. Using pyroxene analyses in Kuroda et al. (1978) for a boninite from Chichi-jima in the Bonin Islands (plotted on Fig. 7A), I calculated an upper temperature of crystallization of 1136°C. Crawford (1980) calculated a range of 1300°C to 1150°C for 15 pairs of crystals in a cumulate clinoenstatite-bearing olivine pyroxenite sill in Victoria, Australia, using the Wells (1977) modification of Wood and Banno's equation. This particular boninitic material appears to be derived from an extremely refractory source, since Ti, Ca, Al, and Na are extremely low, lower than in any of the other examples cited here. The similar range of crystallization temperatures of the Site 458 lavas and the Australian sill result from nearly identical compositions of both pyrox-

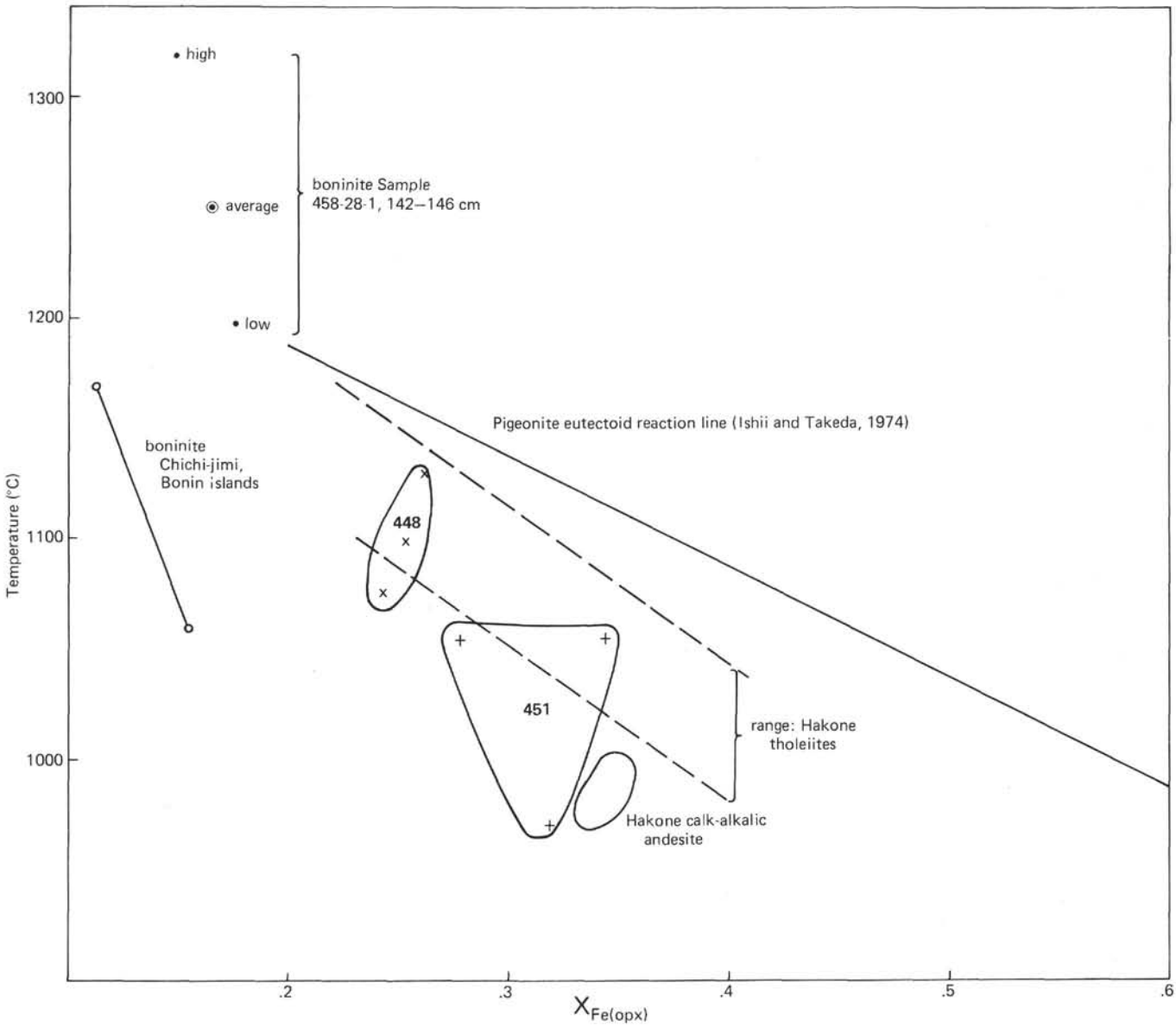

Figure 9. Temperatures of crystallization of coexisting orthopyroxene and clinopyroxene in western Pacific island arc lavas drilled during Legs 59 and 60, plotted against $X_{Fe(opx)}$(= Fe/Mg + Fe in the orthopyroxene). Diagram and Leg 59 data from Ishii (1980). Fields are for Site 448 (Palau-Kyushu Ridge) and Site 451 (West Mariana Ridge) drilled during Leg 59. Boninites plotted are Sample 458-28-1, 142–146 cm of this study (high, low, and average temperatures computed from data of Table 3) and Sample B1, boninite center of pillow, Tsuri-hama, Chichi-jima, Bonin Islands (Kuroda et al., 1978, tables 2 and 4). The difference in temperature of crystallization results from differences in augite compositions (Fig. 7A). Both boninites plot at temperatures as high as or higher than arc tholeiites and calc-alkalic andesites from Sites 448 and 451, as well as from Hakone volcano, Japan.

enes in the two sets of samples. The lower computed temperatures for the marianite and the Chichi-jima sample result primarily from their having more iron-rich augites (Fig. 7A); coexisting bronzites have nearly identical compositions in all the suites. The result of this is that the seemingly more fractionated olivine-free boninitic lavas of Hole 485 have high-temperature pyroxenes similar in composition to those in some extremely refractory boninites carrying olivine and clinoenstatite (the Australian sill). But other lavas which are mineralogically less fractionated, the olivine- and clinoenstatite-bearing marianites of Sharaskin et al. (1980), have lower-temperature bronzite–augite pairs than the Hole 458 boninites. Evidently, the occurrence of neither clinoenstatite nor olivine has much relationship to the temperatures of crystallization of augite and bronzite in these lavas.

The cause of this seemingly contradictory state of affairs is not obvious. The calculations for the marianite and Chichi-jima sample were based on limited published microprobe data (the most magnesian of only two or three bronzite–augite pairs apiece were used). A more thorough data set might have produced more consistency among the calculated temperatures for the various boninites. Probably, however, the compositional differences among the augites are genuine and result from

inherent compositional differences in the host magmas which affect both the shape of the pyroxene solvus in these magmas and the extent of the resulting pyroxene miscibility gap. A fundamentally higher Mg/Mg + Fe ratio for a given Ca abundance in the Hole 458 lavas, for example, might have been involved. This would be difficult to establish because of the effects of alteration. Alternatively, the abundance of minor components such as Na_2O, TiO_2, or volatiles might be responsible. Ishii (1980), for example, has concluded that elevated $p(H_2O)$ among calc-alkalic lavas (such as those of Hakone volcano on Fig. 9) produces lower calculated temperatures of pyroxene crystallization at a given value of X_{Fe} (the ratio Mg/Mg + Fe in orthopyroxenes) than among arc tholeiites. This result, too, is a consequence of more iron-rich clinopyroxenes coexisting with orthopyroxenes of a given X_{Fe} than in the arc tholeiites. On this reasoning we could speculate that the Hole 458 and Australian sill samples were less hydrous than the marianites or Chichi-jima boninites.

These possible complications aside, boninitic lavas in general appear to have been high-temperature melts, with the lowest calculated temperatures of pyroxene phenocryst crystallization still as high as the maximum calculated by Ishii (1980) for magnesian arc tholeiites with olivine and bronzite. This is consistent with the refractory compositions of the mantle sources for boninites inferred from their overall compositions and with the occurrence of extremely magnesian olivine (Fo_{92-94}) and chrome-rich magnesiochromite in some of them (e.g., Cameron et al., 1979, 1980; Crawford, 1980). This, coupled with low Na_2O, TiO_2, CaO, and depleted rare earth element abundances (Wood et al., this volume; Hickey and Frey, this volume), indicates mantle sources that have already undergone previous episodes of melting. Crawford (1980) invoked the two-stage melting hypothesis of Duncan and Green (1978) to explain the boninite–arc tholeiite association such as that found at Site 458. Rather than anhydrous melting, however—which produces contemporaneous MgO-rich and MgO-poor lavas such as komatiites and tholeiites—it is melting that occurred under hydrous conditions which produces the boninites. This has the important petrological effect of allowing silica-saturated residual melts to be derived from olivine normative parents (that is, allowing the olivine–orthopyroxene reaction relationship, which is actually observed in olivine-bearing boninites, to occur; e.g., Crawford, 1980). It also allows melting to occur at geologically reasonable temperatures. Crawford (1980) felt that the peridotite melting experiments under hydrous conditions of Mysen and Kushiro (1977) produced reasonable analogs to boninites at temperatures of 1500–1600°C and pressures of 20 kbar. The experiments were performed on a garnet lherzolite with 1.9% H_2O in the charges. The range of temperatures at which melting occurred was also consistent with the rather high temperatures of crystallization of pyroxenes calculated by Crawford to have occurred upon injection of his sill.

At odds with this, however, are experimental results on the melting behavior of basalts and andesites at elevated $p(H_2O)$. Kuroda et al. (1978) cite the experiments of Yoder and Tilley (1962) on basalts and of Eggler (1972) on andesites to argue that boninite melting temperatures need only be 1000–1100°C at $p(H_2O)$ of 5–10 kbar. Similarly, the liquidus temperatures of a magnesian andesite (Kushiro and Sato, 1978) and a boninite from Hole 458 (Kushiro, this volume) drop to values as low as these at similar water pressures. The latter experiments were done with 12–16% H_2O in the capsules to insure conditions of water saturation at elevated pressures. Between 8 and 14.5 kbar, clinopyroxene in the Hole 458 boninite was the experimentally produced liquidus phase at temperatures of only between 1025°C and 1075°C. The upper value is less by nearly 55° than the lowest value I have calculated for any boninite and is less by 175° than the average value calculated for the pyroxenes of the Hole 458 sample listed in Table 3. If the calculated temperatures of crystallization are correct, they cast into serious doubt the validity of the conditions of melting simulated by the experiments. It seems unavoidable to conclude that melting of boninites is *not* accomplished under water-saturated conditions at elevated pressure. However much water may have facilitated melting, it did not suppress it by the nearly 500° indicated by the difference between melting temperatures of "damp" garnet lherzolite (Mysen and Kushiro, 1977) and those suggested by water-saturated experiments done on the actual lavas. Clearly the precise conditions of boninite melting, and the phase relationships that existed during that melting, are poorly constrained experimentally. Accurate statements about geothermal gradients, other than that they were probably high, are not yet possible.

CLASSIFICATION OF THE BONINITE SERIES

Classifications of island arc magmas have been based either on mineralogy or chemistry. As examples of the former, the pigeonitic and hypersthenic suites of Kuno (1968) come to mind. Their approximate chemical equivalents are the island arc tholeiite series of Jakeŝ and Gill (1970) and the calc-alkalic series of Peacock (1931) and many subsequent workers. As discussed earlier, the boninitic lavas of Hole 458 are not petrographically equivalent to many boninites previously described. For this reason, Meijer (1980) and Meijer et al. (this volume) have proposed a chemical classification that includes in a boninite series both the Hole 458 rocks and previously described boninites. Because the Hole 458 samples lack olivine and clinoenstatite, however, and because they are more evolved than lavas which carry these minerals, the Leg 60 shipboard party elected to call these rocks "high-MgO bronzite andesites" in the site chapters and in other chapters of this volume. This term denotes both the chemical and petrographic features of the Hole 458 lavas.

However, it is obvious that the fundamental mineralogic and petrographic features of the Hole 458 lavas and other boninites are nearly identical. Moreover, the compositions of bronzites and augites in the rocks described from Hole 458 are also nearly identical to those in other boninites, notwithstanding the lack of olivine and clinoenstatite. Some of them also have MgO contents approaching those of boninites from other local-

ities. Others, though, have MgO contents so low (less than 4.5%) that they should not be grouped with rocks described as "high MgO."

I propose that the earlier described examples of boninite series lavas which contain olivine and clinoenstatite be termed *olivine boninites* and that the Hole 458 lavas be called *boninites* to emphasize that they lack olivine. The distinction would be analogous to the terms *olivine tholeiite* and *tholeiite* for the Hawaiian petrographic province (Macdonald and Katsura, 1962, 1964). Bronzite-bearing lavas with a high modal proportion of plagioclase and quartzose segregations in coarse-grained samples could then be described as *bronzite andesites* without concern for the abundance of MgO. At Hole 458, by this terminology, lavas range from boninites to bronzite andesites, with the boninites being the comparatively MgO-rich lavas of Cores 29, 39, and 40 (Fig. 2) and the bronzite andesites the massive lavas of Cores 32–34. Intermediate lavas could be termed *boninitic andesites*, in a manner analogous to *basaltic andesites*. These distinctions have the advantage of utilizing a simple mineralogical modifier to express real differences in chemical composition but leaving no doubt as to the magma type. They also avoid potential confusion with high-MgO andesites not related to boninites, such as those described from the Aleutian arc (Kay, 1978) and Japan (Kushiro and Sato, 1978).

Other members of the boninite magma series described elsewhere include, at the mafic end, marianite, which is basically an olivine boninite rich in clinoenstatite (Sharaskin et al., 1980), and at the silicic end, bronzite or hypersthene dacite (Kuroda et al., 1978). Among known examples of all these lava types, however, geochemical relationships are complex, implying a diversity of mantle source compositions and melting conditions in the mantle (e.g., Hickey and Frey, this volume; Meijer, 1980). Probably no complete cogenetic boninite fractionation series has yet been sampled.

RECOGNITION OF NONGLASSY BONINITE

From the preceding discussion, criteria for the identification of boninites in thin sections which are free of glass can be summarized. The most important criteria are (1) the occurrence of bronzite ± clinoenstatite microphenocrysts ± olivine; (2) the occurrence of augite–bronzite microphenocryst intergrowths and, perhaps additionally, intergrowths involving bronzite, clinoenstatite, and olivine; and (3) the occurrence of tabular or skeletal augite microlites, surrounded by later-grown, and usually finer-grained, plagioclase. Of these criteria, the third is probably the most universal, since, as we have seen, olivine and clinoenstatite phenocrysts do not occur in all boninites, bronzite microphenocrysts may be rare, and bronzite–augite intergrowths are not nearly so common in coarse-grained as in fine-grained and glassy boninites. It is this third criterion which clearly distinguishes boninites from both basalts and typical calc-alkalic andesites, since groundmass plagioclase crystallizes first in both these rock types. The effect of high cooling rates near pillow margins amplifies the textural contrast between basalts and boninites. Whereas in most abyssal tholeiites, particularly those with olivine, the effect of extreme undercooling is first to suppress altogether clinopyroxene crystallization next to glassy rims, in boninites it is plagioclase crystallization that is first suppressed. In both rock types, as undercooling increases toward pillow rims, crystals change morphology from granular and euhedral to skeletal and finally to spherulitic forms. Minerals that form late in an equilibrium crystallization series progress through this sequence before minerals that form early. In basalts, this progression occurs to clinopyroxene before it does to plagioclase; in boninites, it occurs to plagioclase before it does to clinopyroxene.

This contrast can be shown diagrammatically on schematic plots of temperature versus cooling rate. For the case of a Hole 458 boninite (Fig. 10A), the curves show the relative temperatures at which minerals crystallize at different cooling rates. The left side of the diagram corresponds to equilibrium temperatures of crystallization. Following each curve to lower temperature and higher cooling rates, there are systematic changes in crystal morphology. At the left, along each curve, crystals are granular or euhedral, toward the midpoint of each curve they are skeletal, and toward the bottom they are spherulitic or, in some cases, dendritic. At any given cooling rate, corresponding to a particular distance from the edge of a pillow or other cooling unit, a line traced upward from the bottom of the diagram intersects the mineral curves at different points; hence the crystals assume different morphologies. Put another way, at any given cooling rate, the undercooling for, say, clinopyroxene, given by the difference between its equilibrium temperature of crystallization (the left side of the diagram) and its actual temperature of crystallization, is less than for plagioclase. At cooling rates corresponding to spherulitic plagioclase, then, clinopyroxene forms skeletal or dendritic microlites, and magnetite does not crystallize at all. At cooling rates corresponding to spherulitic clinopyroxene, neither magnetite nor plagioclase forms.

For comparison, a similar plot for a Mid-Atlantic Ridge aphyric olivine tholeiite is shown on Figure 10B, from Kirkpatrick (1978). The same general variations in morphologies apply, but the contrasts with boninites are that the plagioclase and clinopyroxene curves are switched, and olivine occurs instead of orthopyroxene. The various crystallization zones of Table 2 are summarized on Figure 10A. The corresponding basalt crystallization zones of Kirkpatrick (1978) are summarized on Figure 10B. Together, Figure 10A and Table 2 constitute a general petrographic description for pillowed boninites. Somewhat different relationships would prevail for olivine boninites or marianites. For bronzite andesites, the clinopyroxene and plagioclase curves of Figure 10A would be closer together.

COMPOSITIONAL AND KINETIC CONTROLS ON BONINITE CRYSTALLIZATION

Although many workers have discussed the mechanism by which boninitic melts can be derived from the mantle, little attention has been given to how those melts

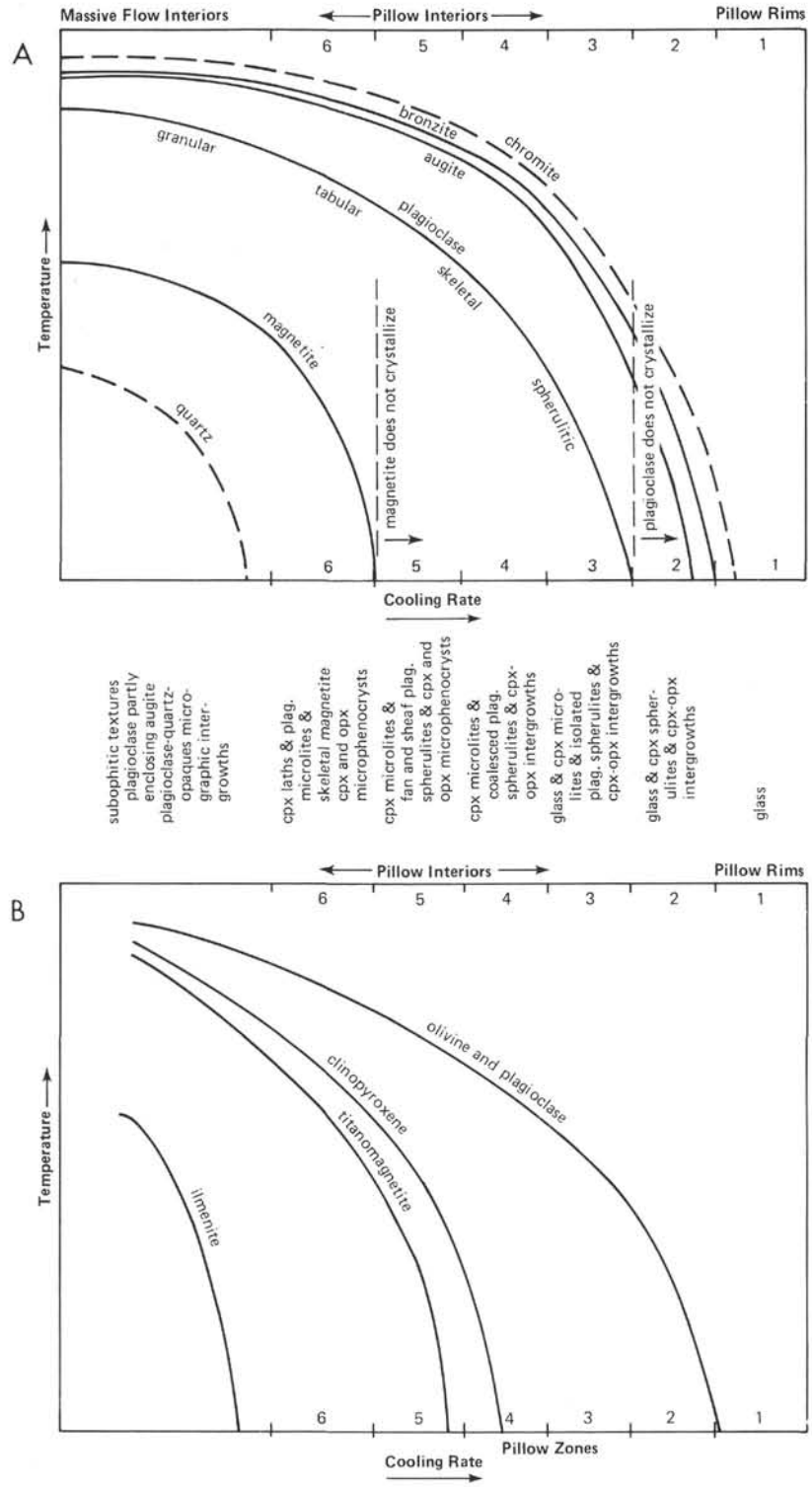

Figure 10. A. Schematic diagram showing deviations from the sequence of equilibrium crystallization temperatures (left side of diagram) for minerals in Hole 458 boninite as cooling rate is increased (to the right). The pillow zones of Table 2 are summarized at the bottom of the diagram. The generalized changes in crystal morphologies for plagioclase are shown next to that curve. Similar variations occur with the other minerals, and in the same order, although not necessarily along precisely the same portions of their curves. B. A similar diagram for a Mid-Atlantic Ridge olivine tholeiite from DSDP Site 396, after Kirkpatrick (1978). His pillow zones are indicated on the diagram.

produce the peculiar mineralogies and textures of boninites. It seems obvious that crystallization of orthopyroxene rather than olivine results from combining high SiO_2 with high MgO and Mg/Mg + Fe (e.g., Dallwitz et al., 1966; Dallwitz, 1968; Crawford, 1980). It is not so obvious why clinopyroxene crystallizes ahead of plagioclase. The explanation appears to be related to high SiO_2/Al_2O_3 and low CaO/Al_2O_3 in boninitic magmas. The latter ratio averages 0.63 in Chemical Type A_1 boninitic lavas of Hole 458 and 0.59 in Type A_2 boninites (calculated from data in Wood et al., this volume). Cameron et al. (1979) cite CaO/Al_2O_3 in some boninites as low as 0.55. Similarly, the marianites of Sharaskin et al. (1980) have CaO/Al_2O_3 ranging between 0.40 and 0.63, with an average of 0.55. These compare with ratios between 0.75 and 0.88 in typical basalts and in fact more closely resemble values in andesites than in basalts. The result of this is a propensity for boninitic magmas to crystallize comparatively anorthite-poor (and thus lower-temperature) plagioclases, in spite of having very magnesian and high-temperature pyroxenes. Bougault et al. (this volume) report plagioclases in Hole 458 boninites with SiO_2 between 50% and 54% and ranging in composition between An_{77} to An_{63}. These are similar to plagioclase compositions in fractionated basalts with lower Mg/Mg + Fe than boninites.

A fair approximation to phase relations in the Hole 458 boninites is the system diopside-albite-anorthite (Bowen, 1915), and it can be used to illustrate the contrast between basalts and boninites shown on Figure 10. Boninite compositions would correspond to those on the diopside side of the cotectic boundary separating the diopside and plagioclase fields (Fig. 11). Basalts would correspond to compositions on the plagioclase side. Any liquid with less SiO_2 and higher CaO/Al_2O_3 than boninites would correspond to compositions closer to the anorthite corner of the diagram—that is, away from the diopside field—and would more closely resemble basalts. Compositions analogous to boninites in this system first crystallize diopside. Fractionation shifts residual liquid compositions away from the diopside apex until the plagioclase–diopside cotectic is reached, whence both minerals crystallize together. With basalts, plagioclase crystallizes first, until residual liquids reach the same cotectic boundary, and both plagioclase and diopside crystallize together.

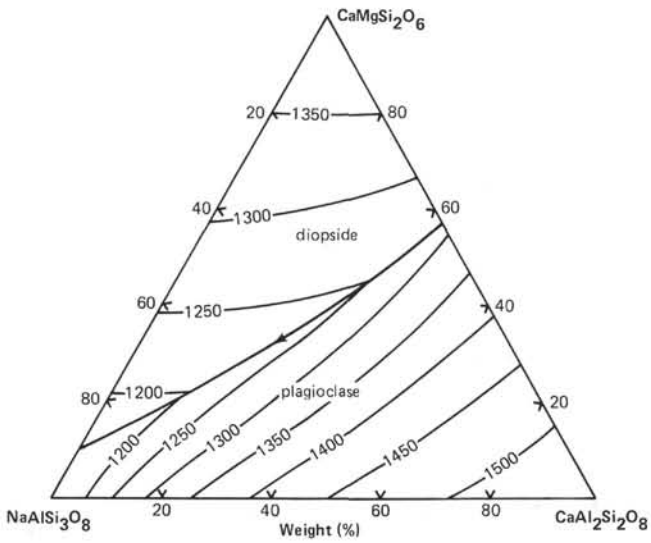

Figure 11. Projection of the liquidus surface of the system Di-An-Ab at 1 atm (Bowen, 1915; Kushiro, 1972b). The contrast between boninite and basalt crystallization sequences (Fig. 10) is approximated by the difference in crystallization sequences between compositions plotting on opposite sides of the cotectic boundary, boninite in the diopside field, basalts in the plagioclase field.

High volatile contents, particularly the concentration of H_2O in the melt, might be thought to hinder the crystallization of plagioclase, inasmuch as the liquidus curve in the system Ab–An is known to drop in temperature at elevated $p(H_2O)$ (Yoder, 1969; Johannes, 1978). Meijer et al. (this volume) alluded to this possibility in consideration of the crystallization of plagioclase spherulites in Hole 458 boninite glasses. For such an effect to be appreciable, however, drops in water pressures of several kilobars would be required. Yoder (1969) documented a shift of the cotectic boundary shown on Figure 11 toward the anorthite corner at water pressures of 5–10 kbar. However, we are dealing with minerals which formed in lavas extruded under no more than 3000–4000 meters of water, and probably less. Judging from Yoder's data, this might change the sequence of mineral crystallization if the original melt composition were very close to the cotectic boundary to begin with. In my view, the compositional differences between boninite and basalt must be much more important than the concentrations of volatiles in explaining observed mineralogical and textural differences between the two. Basalts of the Mariana Trough such as those cored at Site 454 during Leg 60, for example, are quite vesicular. Basalts dredged from the center of the Trough have mainly water in vesicles trapped in glass (Garcia et al., 1979). These basalts were all erupted in water depths of about 3500 meters, yet all have typical basalt textures and mineralogies. None have experienced a reversal in the plagioclase–clinopyroxene crystallization sequence.

There are two terrestrial lava types with textures similar to boninites of which I am aware. Cameron et al. (1979, 1980) have pointed out textural and compositional similarities between boninites and Archean basaltic komatiites, although they stress that the latter were generated under nearly anhydrous conditions. Like boninites, the basaltic komatiites they describe have augite microlites and two-pyroxene intergrowths, but no plagioclase, in glassy samples. But they are much more olivine-rich and have CaO/Al_2O_3 ratios of about 0.8, similar to values in basalts. The appearance of clinopyroxene before plagioclase in these basalts must be related only to their high MgO and low SiO_2 rather than low CaO/Al_2O_3. On Figure 11, they would be approximated by compositions in the diopside field but closer to the diopside–anorthite side of the diagram than boninites.

The other terrestrial lava type with some textures similar to boninites is submarine examples of the nephe-

linite series of oceanic volcanoes, namely basanites and olivine nephelinites. Pillows of these compositions have been dredged from a number of places, including the Line Islands seamount chain (Natland, 1976). These carry (altered) olivine phenocrysts and abundant titan-augite microlites, but no plagioclase, in glassy samples. In these lavas, suppression of plagioclase crystallization stems from low abundances of both SiO_2 and Al_2O_3. The lavas are highly undersaturated with respect to SiO_2, partly also because of high alkali contents, hence cannot crystallize orthopyroxene. Although the system Di-Ab-An is a rather poor analog for such rocks, on Figure 11 they would be approximated by compositions also in the diopside field but closer to the diopside–albite side than boninites.

One other close textural analog to boninites is the group of lunar quartz-normative, pyroxene-phyric basalts mentioned earlier and described by Dowty et al. (1974). In those rocks, phenocrysts are pigeonite (rather than bronzite) and augite. Augite microlites are abundant, and plagioclase is absent in glassy samples. In coarser-grained samples, plagioclase crystallizes well after the appearance of both pyroxenes, and its nucleation drastically modifies all subsequent pyroxenes to much less calcic compositions. These basalts experienced extreme cooling rates upon extrusion onto the surface of the lunar maria, cooling rates matched naturally by few circumstances on the Earth's surface other than submarine pillow eruption. Like the boninites, these lunar basalts have augite overgrowths on low-Ca pyroxenes (pigeonite), which tend to have skeletal morphologies in glassy samples. Coarser-grained samples of these lunar basalts even contain ferroaugite and subcalcic ferroaugite, some of which have compositions similar to pyroxenes in the boninite studied by Bougault et al. (this volume), shown on Figure 7C. The lavas are considerably richer in iron and TiO_2 than boninites, however, and contain virtually no water. As a result, even the initial pyroxenes to form were comparatively iron-rich magnesian pigeonites, not bronzites, and ground-mass iron and titanium enrichments were extreme, leading to formation of interstitial metallic iron and ilmenite.

In an effort to model the crystallization of these lunar pyroxene-phyric basalts, Dowty (1980) applied numerical techniques to natural composition and the synthetic composition $Di_{60}An_{30}Ab_{10}$ that plots in the diopside field of Figure 11. His results bear on one aspect of the textures in the Hole 458 boninites: the high modal proportion of clinopyroxene in glassy samples. Dowty considered two cases: crystallization under conditions of constant decrease of temperature (1 deg/hr) and conditions of constant loss of heat (0.001 cal/s). Different effects were observed in the two cases, but in both the liquid composition overshot the cotectic so that diopside continued to crystallize even after the liquid was well into the plagioclase field. In effect, the duration of the period of diopside crystallization was extended, and that of plagioclase diminished, by rapid cooling rates. Plagioclase began to crystallize only when the critical undercooling necessary for its nucleation was reached. This type of phenomenon would explain, for example, the increase in Al contents of clinopyroxenes in Hole 458 boninites (Figs. 7A and 8) and the siliceous, essentially dacitic composition of the glass from the same sample (Table 4, column 1). The modeling also suggested that the initial stages of crystallization should be dominated by homogeneous or quasi-homogeneous nucleation, which would produce mainly individual crystals with a limited range in size (i.e., the clinopyroxene microlites of Fig. 4). In olivine tholeiites, however, so many plagioclase crystals have formed by the time clinopyroxene crystallizes that nucleation of pyroxene is primarily heterogeneous, producing rows of parallel and closely spaced dendrites with faceted crystal terminations, all attached at their other ends to earlier-formed crystals (see Natland, 1980, fig. 5B).

A final question concerns the development of porphyritic texture in the Hole 458 boninites. Until recently, conventional wisdom held that porphyritic texture was a consequence of two or more stages of cooling. But there is now fairly considerable evidence that porphyritic texture can be produced by a single-stage cooling event (i.e., cooling at constant rates; see summary by Lofgren, 1980). The critical requirement is that the magma not be multiply saturated—that is, that the liquidus phase be modally dominant and crystallize by itself before introduction of any other modally significant phase, as, for example, augite before plagioclase in boninites. When the second phase finally begins to crystallize, so many nuclei form that the sizes of new crystals of the first phase decrease abruptly, producing a rock with two sizes of that mineral. The composition of that mineral may also change abruptly when a second phase nucleates (Dowty et al., 1974).

In glassy Hole 485 boninites, however, there are two sizes of clinopyroxene crystals, but there is no plagioclase. The larger crystals include blocky augite glomerocrysts, isolated augite phenocrysts, and augite–bronzite intergrowths. These are surrounded by myriads of smaller augite microlites set in glass. The glomerocrysts and intergrowths suggest types of heterogeneous nucleation, whereas the microlites probably formed homogeneously. Their period of growth coincided with that of the growth of dendritic projections on the phenocrysts. At least two stages of cooling are thus implied.

In fact, there were probably more than two stages of cooling, which may have influenced phenocryst growth. The lavas themselves had to undergo a series of abrupt increases in cooling rate, corresponding to periods of ascent into the shallow crust, eruption, large-scale flow of lava, and budding of pillows. Because pillows form from each other, a given packet of lava may have squirted through several pillows before finally freezing, undergoing at each pillow a change in cooling rate. The specific cooling histories of different packets of lava during these later stages of eruption will thus vary. That the phenocrysts in the Hole 458 boninites formed during these later stages of eruption is evident from their variety in any given sample, the different forms they take from sample to sample, and their apparent absence in the coarsest-grained boninites. Put another way, there is

no population of phenocrysts common to all samples that appears to be left over from any large holding reservoir or magma chamber. The simplest form of the two-stage cooling hypothesis has phenocrysts forming in magma chambers, and in the groundmass upon eruption. That did not occur here.

In summary, the crystallization sequence of boninites is determined primarily by their chemistry, but their textures, modes, crystal morphologies, and mineral compositions are dictated in large measure by kinetic factors. There are several other lava types whose crystallization at high cooling rates is more or less analogous to that of boninites. Laboratory experiments and modeling promise to improve our understanding of the crystallization of all these rocks.

CRYSTAL MORPHOLOGIES IN BASALTS OF HOLES 458 AND 459B

Basalts of arc tholeiite composition interbedded with boninites in Hole 458 are for the most part intensely altered and fractured. Glassy and spherulitic zones were especially vulnerable to alteration, hence were either not recovered during coring or were totally reconstituted to clays. Available thin sections made on board ship are of altered hyalopilitic samples, with small acicular plagioclase microlites set in groundmasses either completely transformed to clays (Fig. 12A) or retaining traces of spherulitic clinopyroxene and opaque minerals (Fig. 12B).

In the basalts of Hole 459B as well, alteration is intense, and the outermost glassy and spherulitic zones were not recovered. Two types of basalt were cored, coarse-grained massive rocks of Lithologic Units 1 and 3 (Fig. 2) and fine-grained pillows in Lithologic Units 2 and 4. Some finer-grained spherulitic rocks occur at the top of Lithologic Unit 1 and may represent the upper chilled margin of this 29-meter-thick flow. Despite there being two major and several minor chemical subdivisions among the basalts, petrographic distinctions are not easy to make, owing to the combined effects of scarcity of phenocrysts, similarity of groundmass textures among the different lithologic units, and alteration. The two B_1 basalt subtypes (Fig. 2) are relatively richer in MgO and poorer in iron (as Fe_2O_3) than the B_2 subtypes (Wood et al., this volume), but this appears to be reflected mainly in a higher proportion of clinopyroxene, and somewhat less titanomagnetite, in the rocks. All the basalts appear to be saturated in both clinopyroxene and plagioclase, hence would be represented by cotectic crystallization on Figure 11.

The finest-grained basalts in Hole 459B are hyalopilitic, with acicular microlites of both plagioclase and clinopyroxene in an altered mesostasis (Fig. 12C). The pyroxenes are pale brown in color, and both minerals are usually surrounded by fuzzy spherulitic overgrowths. The plagioclase microlites flare into spherulitic terminations at either end.

Other somewhat more crystalline samples are quite vesicular (Fig. 12D), with scattered plagioclase microlites separating into two arms at the ends of many crystals. These are surrounded by finer-grained spherulitic sheafs of clinopyroxene. Closer inspection of these reveals them to be bundles of individual pyroxene fibers typically splaying from larger elongate crystals which might be termed "core fibers" (Fig. 12, E and F). Cubic and octahedral titanomagnetite grains cluster around the edges of these bundles.

Examples of the coarsest-grained pillow basalts are shown in Figure 12, G and H. These are weakly vesicular, suggesting that basalts with abundant vesicles are confined to narrow zones close to pillow margins. Vesicles that occur in the coarser-grained samples, though rare, are often large and concentrated into trains (Fig. 12H). Plagioclases in the coarser-grained portions of pillows are elongate crystals, many of them separating at their ends into two dendritic arms, a consequence of heightened undercooling (e.g., Kirkpatrick, 1978). In Figure 12G these are surrounded by bundles and clusters of spherulitic clinopyroxene. Overall, these rocks can be described as having mesh textures, with abundant relatively short crystals rather than fewer longer crystals; hence they appear to have had many centers of nucleation. This indicates cooling from somewhat below rather than somewhat above liquidus temperatures (Walker et al., 1979; Lofgren, 1980).

An interesting feature of hyalopilitic samples is that several contain segregation vesicles lined with dark reddish brown devitrified glass and containing elongate opaque minerals (Fig. 13A and B). The glass is made up of fine spherulitic material of optically indeterminant origin. The crystallization of titanomagnetite before plagioclase and clinopyroxene in these vesicles is a reversal of the crystallization sequence elsewhere in the rocks, and probably indicates elevated oxygen fugacities in the vesicles.

Phenocrysts are rare in these basalts. Two examples are shown in Figure 13, C and D. The first, in a rather coarse-grained sample, is a cluster of intergrown euhedral augites. The second is an irregular isolated augite that may be a xenocryst or a type of skeletal crystal; it has a narrow reddish outer zone. Tabular plagioclase microphenocrysts also occur but are very rare.

The massive flows of Cores 66–68 in Hole 459B have coarsely subophitic or intergranular textures in their interiors. Alteration is not as pervasive in these basalts as in the pillows and typically consists of clay minerals (smectites and celadonite) lining cavities and replacing plagioclase and augite (Natland and Mahoney, this volume). *In situ* magmatic differentiation has been locally extensive in these massive rocks, producing micrographic intergrowths of quartz and two feldspars (Fig. 13, E and F) and locally coarse patches of quartz (Fig. 13, G and H). Some of the micrographic intergrowths have a distinctively spherulitic texture, with the intergrown feldspar splaying from the ends of larger plagioclase euhedra (Fig. 13F). One can speculate that these late-stage textures resulted from increased viscosity of the silicic residual liquids, reducing diffusion rates in the melt relative to crystal growth, hence promoting growth of spherlites. More conventional interpretations of micrographic intergrowths are (1) that they represent eutectic crystallization of quartz and alkali feldspar (Vogt, 1921) and

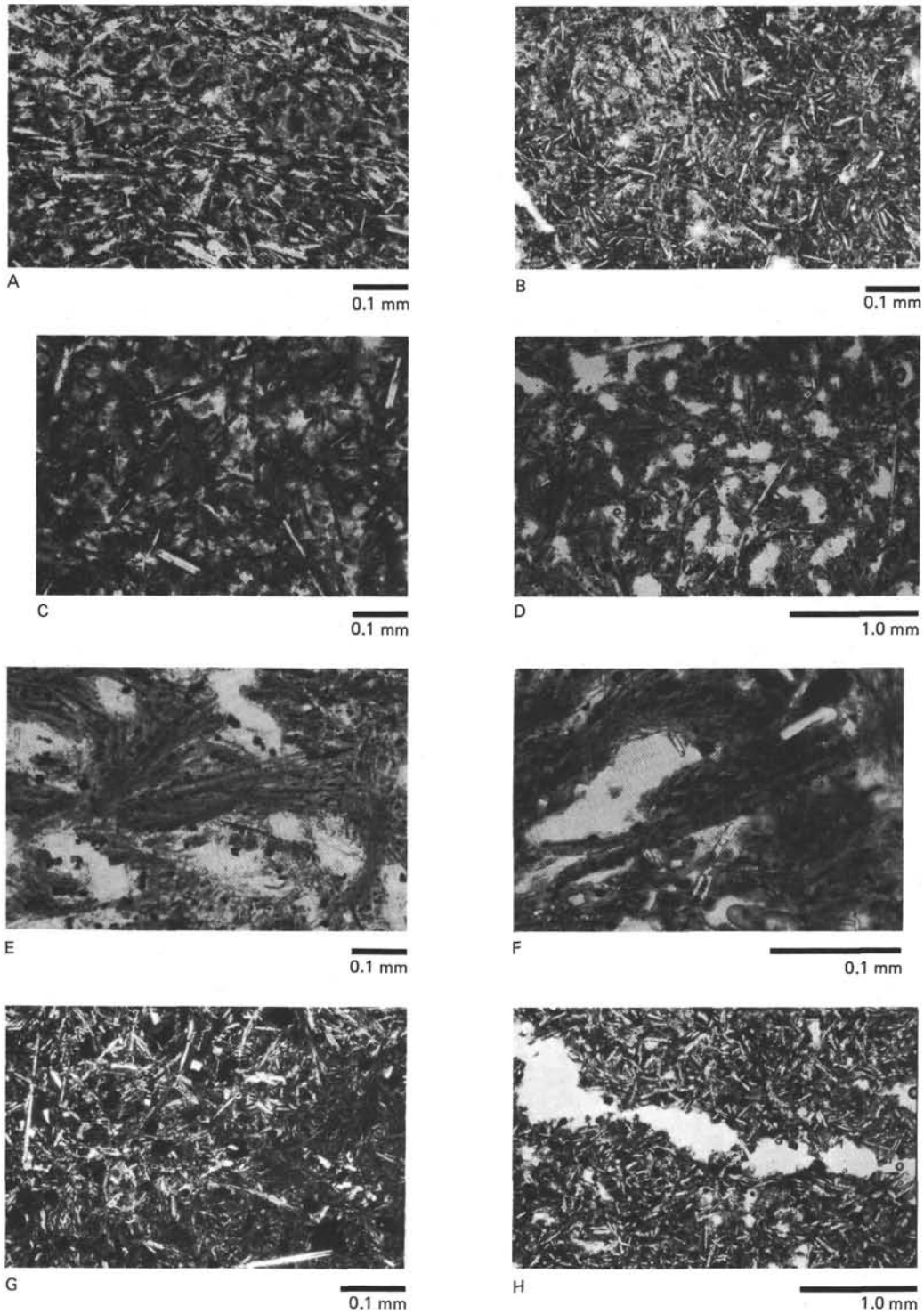

Figure 12. Petrographic features of tholeiitic basalts, Holes 458 and 459B. A. Sample 458-46-1, 78–80 cm. Plagioclase microlites in an altered, formerly glassy mesostasis. Plane light. B. Same sample as A, also plane-polarized light. Titanomagnetites are fairly abundant at lower right. C. Sample 459B-63-1, 24–27 cm. Plagioclase microlites with spherulitic overgrowths in an altered glassy mesostasis. Plane light. D. Sample 459B-60-1, 44–47 cm. Plane light. Chemical Subtype B_{1A}. Microlites of plagioclase and spherulitic clinopyroxene in a vesicular basalt. E and F. Same sample as D, both in plane light. Examples of branching spherulitic clinopyroxene, speckled with titanomagnetite. G. Sample 459B-71-1, 31–33 cm. Plane light. Plagioclase microlites and clinopyroxene spherulites in a Type B_2 basalt. Dark spots are clumps of titanomagnetite with outlines obscured by alteration. H. Same sample as G, plane light, showing portion of a train of vesicles.

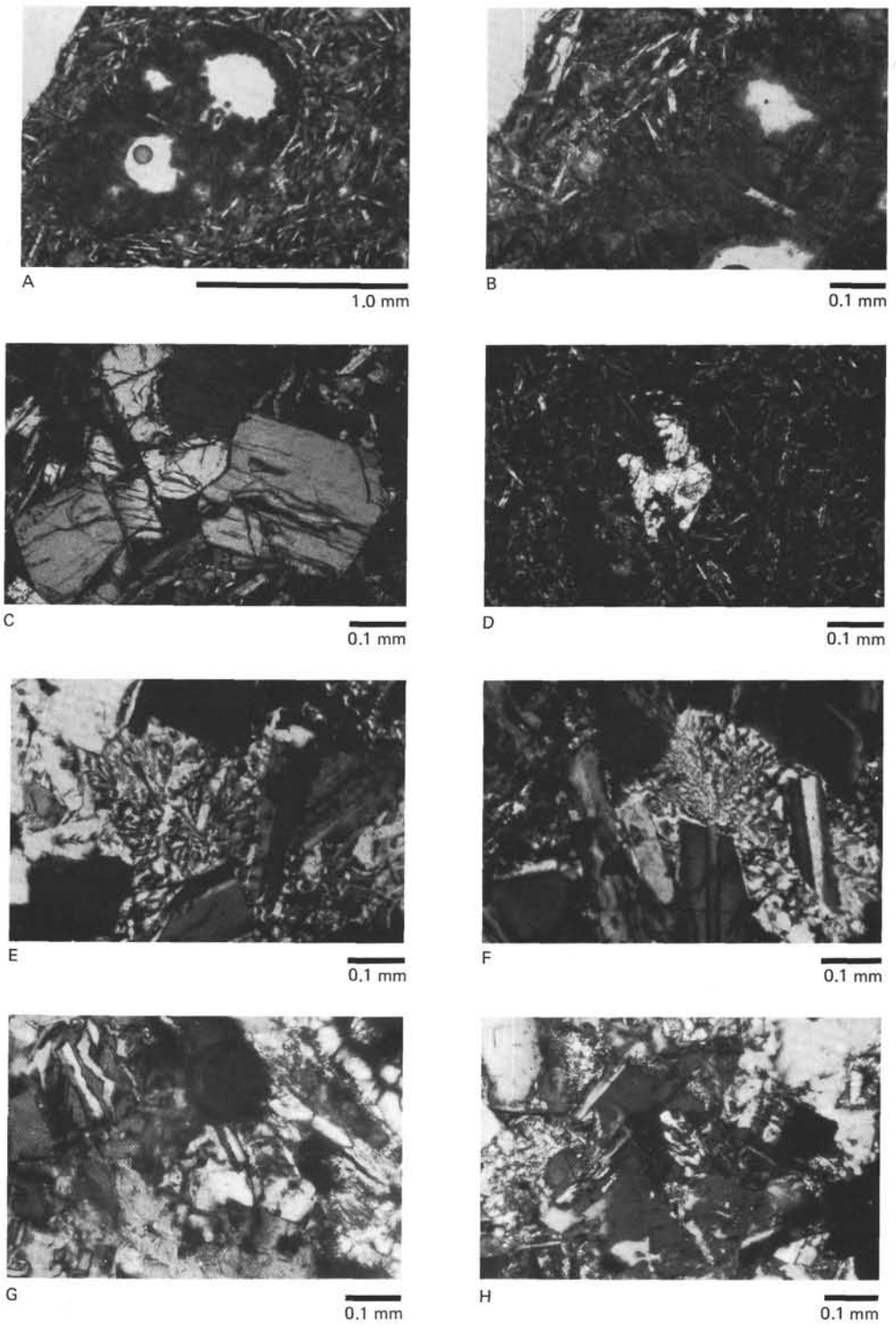

Figure 13. Segregation vesicles, phenocrysts, and quartz-feldspar intergrowths in coarse-grained tholeiitic basalts, Hole 459B. A. Sample 459B-10-1, 69–71 cm, plane light. A segregation vesicle in hyalopilitic basalt with plagioclase microlites. B. Detail of A, showing abundant elongate skeletal titanomagnetite in segregation vesicle, surrounded by very fine spherulitic material. C. Sample 459B-60-2, 96–99. Crossed nichols. Intergrowth of several euhedral augite phenocrysts, in a finer-grained subophitic matrix. D. Sample 459B-63-1, 81–83 cm. Crossed nichols. Irregular single augite microphenocryst in hyalopilitic basalt. E–H. Sample 459B-66-3, 3–4 cm. Crossed nichols. E and F show patchy intergrowths of a more calcic plagioclase (generally darker and twinned) and a less calcic plagioclase (lighter), with F particularly showing spherulitic morphology extending from the large upright plagioclase at lower center. G and H show patchy quartz (low relief, darker at this orientation) intergrown with plagioclase.

(2) that they are produced at elevated $p(H_2O)$ (Luth et al., 1964). In these rocks, however, the feldspar intergrown with quartz is plagioclase (see the following)—that is, it is not potassic, hence eutectic compositions were not reached. Moreover, the experiments of Luth et al. (*loc. cit.*) relate to crystallization at 2–10 kbar $p(H_2O)$ in the granite system, not to late-stage crystallization of basalt flows. Here, the experiments of Fenn (1977a, 1977b), who produced alkali feldspars and albite with coarsely spherulitic morphologies from undercooled silicic melts, seem most relevant, given the observed textures.

COMPARISON OF ARC AND ABYSSAL THOLEIITES

In several respects, these rocks resemble East Pacific Rise and Galapagos Rift ferrobasalts (Natland, 1980) more closely than they do olivine and plagioclase tholeiites of either the East Pacific Rise or the Mid-Atlantic Ridge (Natland, 1978, 1980). The critical points of similarity to the former and contrasts with the latter are (1) lack of olivine phenocrysts; (2) occurrence of clinopyroxene phenocrysts and, more rarely, plagioclase phenocrysts; (3) development of acicular and even equant clinopyroxene crystals in the same spherulitic rocks are acicular and skeletal plagioclases; and (4) abundance of opaque minerals. Regarding the opaque minerals, the intensity of magnetization of some of the finer-grained Hole 459B basalts is the highest ever found in DSDP materials (Bleil, this volume), fully five times greater than the highest intensity recorded among pillow basalts with >15% iron as Fe_2O_3 and 1.9% TiO_2 at the Galapagos Rift (Petersen and Roggenthen, 1980). However, these are not as iron-enriched (see Table 1), indicating that elevated oxygen fugacity may have acted to promote crystallization of titanomagnetite. The Hole 459B arc tholeiites are also more vesicular than eastern Pacific ferrobasalts, a feature perhaps consistent with elevated oxygen fugacity. The early crystallization of titanomagnetite may also have prevented an extreme of iron enrichment in interstitial glass. This probably prevented the extreme darkening of spherulitic zones so prevalent among eastern Pacific ferrobasalts (Natland, 1980) and promoted the development of quartz-normative residual melts that produced so much quartz in the coarser-grained flow interiors (e.g., Osborne, 1958, 1962, 1979). With 56–59% SiO_2, samples from the massive flows of Cores 66–68 have higher SiO_2 and normative quartz (8–10%) than comparably iron-enriched (11–12% as Fe_2O_3) abyssal tholeiites.

PYROXENE AND FELDSPAR COMPOSITIONS

Two clinopyroxene and three plagioclase compositions were obtained from a single sample from Hole 459B during an electron microprobe reconnaisance of clay mineral compositions (described in Natland and Mahoney, this volume). The analyses are listed in Table 5. The sample was from one of the coarse-grained massive flows with quartz-feldspar micrographic intergrowths. The analyzed pyroxenes are the cores of two large augite crystals and resemble augite compositions obtained by Meijer et al. (this volume), as shown on Figure 7D. The plagioclase analyses are of the core and rim of a large euhedral crystal and of a nearby small feldspar grain intergrown with quartz. The large crystal is zoned from calcic labradorite to andesine, and the smaller crystal is calcic oligoclase, containing slightly more structural Or than the larger crystal (Table 5). More alkalic feldspar such as anorthoclase may more generally be intergrown with quartz elsewhere in the rock but has not been analyzed with a microprobe.

The arc tholeiite augites listed in Table 5, as well as those of Meijer et al. (this volume), have greater structural Wo than the boninite augites of Table 3, as shown on Figure 7D. However, some augites in Hole 458 boninites analyzed by other workers in this volume are as calcic as the arc tholeiite augites, as indicated by the larger of the two fields superposed on Figure 7D. A

Table 5. Electron microprobe analyses of pyroxenes and plagioclases, Sample 459B-66-3, 3–4 cm (#1).

	Clinopyroxenes		Plagioclases		
SiO_2	49.31	48.29	50.93	56.89	65.09
Al_2O_3	2.45	2.37	30.64	27.47	24.42
FeO	14.40	14.32	0.81	0.85	0.55
MnO	0.31	0.33	0.01	0.03	0.00
MgO	12.69	12.87	0.13	0.05	0.00
CaO	18.12	17.24	13.49	9.46	5.33
Na_2O	0.16	0.25	3.36	5.54	7.83
K_2O	0.03	0.02	0.03	0.04	0.19
TiO_2	0.48	0.44	0.01	0.06	0.05
	97.95	96.13	99.41	100.34	103.46
	Number of Ions on Basis of 6(O)		Number of Ions on Basis of 32(O)		
Si	1.915 } 2.000	1.911 } 2.000	9.330 } 15.950	10.182 } 15.978	11.119 } 16.037
Al	0.085 }	0.089 }	6.618 }	5.797 }	4.919 }
Al	0.023 }	0.021 }	0.001 }	0.008 }	0.006 }
Ti	0.014 }	0.013 }	0.124 }	0.127 }	0.077 }
Fe	0.468 }	0.474 }	0.001 }	0.005 }	0.000 }
Mn	0.010 } 2.022	0.011 } 2.031	0.036 } 4.010	0.013 } 3.900	0.000 } 3.696
Mg	0.735 }	0.759 }	2.648 }	1.814 }	0.976 }
Ca	0.754 }	0.731 }	1.194 }	1.923 }	2.594 }
Na	0.012 }	0.019 }	0.007 }	0.009 }	0.041 }
K	0.002 }	0.001 }			
	$Wo_{38.6}En_{37.5}Fs_{23.9}$	$Wo_{37.2}En_{38.7}Fs_{24.1}$	$An_{69}Ab_{31}Or_{0.002}$	$An_{48.4}Ab_{51.3}Or_{0.3}$	$An_{27.0}Ab_{71.8}Or_{1.2}$

greater contrast can be seen for most pyroxenes on Figure 8, which plots tetrahedrally coordinated Al versus Ti. Boninitic augite phenocrysts have very low Ti, whereas most of the arc tholeiite clinopyroxenes have considerably higher Ti at comparable Al_Z. The two augites with least Ti from Hole 459B are from Core 60, Chemical Subtype B_{1A}, which earlier was noted as having a nearly boninite composition. Among the boninite augites, only those that mantle bronzite have elevated Ti, but they also have elevated Al_Z and therefore do not overlap the arc-tholeiite augite compositions.

CONCLUSIONS

The two primary aims of this chapter have been (1) to establish a petrographic basis for identifying boninites, whether or not they are glassy, and (2) to outline the various ways in which kinetic factors influence modes, textures, crystal morphologies, and mineral compositions in these pillow lavas. The treatment has been mostly qualitative, and the mineralogical data so far are limited. Nevertheless, several important conclusions can be drawn.

Boninites assuredly have unusual compositions which must be seen as having a major role in determining their mineralogy. However, because the Hole 458 boninites are pillow lavas, rocks with various grain sizes and crystallinity had to be examined before this could become fully apparent. Analogies to laboratory experiments reproducing crystal morphologies and rock textures were required to understand the significance of phenocrysts and the lack of plagioclase in glassy boninites. Surprising textural and mineralogical analogs to boninites exist in nature, particularly the lunar pyroxene-phyric basalts, whose textures have been studied extensively. However, rigorous understanding of boninite crystallization will be realized only when laboratory experiments are carried out on boninite compositions. It will be necessary to conduct these with varying proportions of water, particularly to determine the effect of water on the crystallization temperatures of pyroxenes. In view of the significance of boninites to magma generation in island arcs, the need for further experimentation should be evident.

ACKNOWLEDGMENTS

I am grateful to the crew of marine technicians on board *Glomar Challenger* during Leg 60 for skillful preparation of samples and thin sections. Bill Melson made the time available for me to use the Smithsonian Institution's electron microprobe, and I am grateful to him and to Eugene Jarosewich for assistance in operating the equipment. Sherman Bloomer and Jim Kirkpatrick provided helpful discussion and comments on the manuscript.

REFERENCES

Bloomer, S., Melchior, J., Poreda, R., et al., 1979. Mariana arc-trench studies: Petrology of boninites and evidence for a "boninite series." *Eos*, 60:968. (Abstract)

Bowen, N. L., 1915. The crystallization of haplobasaltic, haplodioritic, and related magmas. *Am. J. Sci.* (4th series) 40:161–185.

Boyd, F. R., and Schairer, J. F., 1964. The system $MgSiO_3$–$CaMg_2Si_2O_6$. *J. Petrol.*, 5:275–309.

Brown, G. M., 1968. Experimental studies on inversion relations in natural pigeonitic pyroxenes. *Carnegie Inst. Washington Yearb.*, 66:347–353.

_____, 1972. Pigeonitic pyroxenes: a review. *Geol. Soc. Am. Mem.*, 132:523–534.

Cameron, W. E., Nisbet, E. G., and Dietrich, V. J., 1979. Boninites, komatiites, and ophiolitic basalts. *Nature*, 280:550–553.

_____, 1980. Petrographic dissimilarities between ophiolitic and ocean-floor basalts. *In* Panyiotou, A. (Ed.), *Ophiolites: Proceedings International Ophiolite Symposium Cyprus, 1979:* Nicosia (Rep. Cyprus Min. Agric. Nat. Resources Geol. Surv. Dept.), pp. 182–192.

Crawford, A. J., 1980. A clinoenstatite-bearing cumulate olivine pyroxenite from Howqua, Victoria. *Contrib. Mineral. Petrol.*, 75: 353–367.

Dallwitz, W. B., 1968. Chemical composition and genesis of clinoenstatite-bearing volcanic rocks from Cape Vogel, Papua: A discussion. *Proc. XXIII Int. Geol. Cong.*, 2:229–242.

Dallwitz, W. B., Green, D. H., and Thompson, J. E., 1966. Clinoenstatite in a volcanic rock from the Cape Vogel area, Papua., *J. Petrol.*, 7:375–403.

Deer, W. A., Howie, R. A., and Zussman, J., 1963. *Rock-forming Minerals 2: Chain Silicates:* New York (John Wiley & Sons).

Dietrich, V., Emmermann, R., Oberhansli, R., et al., 1978. Geochemistry of basaltic and gabbroic rocks from the West Mariana basin and the Mariana Trench. *Earth Planet. Sci. Lett.*, 39:127–144.

Donaldson, C. H., 1976. An experimental investigation of olivine morphology. *Contrib. Mineral. Petrol.*, 57:187–213.

Dowty, E., 1980. Crystal growth and nucleation theory and the numerical simulation of igneous crystallization. *In* Hargraves, R. B. (Ed.), *Physics of Magmatic Processes:* Princeton (Princeton University Press), pp. 419–485.

Dowty, E., Keil, K., and Prinz, M., 1974. Lunar pyroxene-phyric basalts: Crystallization under supercooled conditions. *J. Petrol.*, 15: 419–453.

Duncan, R. A., and Green, D. H., 1980. The role of multistage melting in the formation of oceanic crust. *Geology*, 8:22–26.

Eggler, D. H., 1972. Water-saturated and undersaturated melting relations in a Paricutin andesite and an estimate of water content in the natural magma. *Contrib. Mineral. Petrol.*, 34:261–271.

Fenn, P. M., 1977a. The nucleation and growth of alkali feldspars from hydrous melts. *Can. Mineral.*, 15:135–161.

_____, 1977b. The nucleation and growth of albite from the melt in the presence of excess SiO_2. *Geol. Soc. Am. Abs. with Programs*, 9:973–974. (Abstract)

Garcia, M. O., Liu, N. W. K., and Muenow, D. W., 1979. Volatiles in submarine volcanic rocks from the Mariana island arc and trough. *Geochim. Cosmochim. Acta*, 43:305–312.

Green, D. H., 1976. Experimental testing of "equilibrium" partial melting of peridotite under water-saturated, high-pressure conditions. *Can. Mineral.*, 14:255–268.

Ishii, T., 1980. Pyroxene geothermometry of basalts and an andesite from the Palau-Kyushu and West Mariana Ridges, Deep Sea Drilling Project Leg 59, *In* Kroenke, L., Scott, R., et al., *Init. Repts. DSDP*, 59: Washington (U.S. Govt. Printing Office), 693–718.

Ishii, T., and Takeda, H., 1974. Inversion, decomposition, and exsolution phenomena of terrestrial and extraterrestrial pigeonites. *Mem. Geol. Soc. Jpn.*, 11:19–36.

Jakeš, P., and Gill, J., 1970. Rare earth elements and the island arc tholeiite series. *Earth Planet. Sci. Lett.*, 9:17–28.

Johannes, W., 1978. Melting of plagioclase in the systems Ab-An-H_2O and Qz-Ab-An-H_2O at P_{H_2O} = 5 kbars, an equilibrium problem. *Contrib. Mineral. Petrol.*, 66:295–303.

Johanssen, A., 1937. *A Descriptive Petrography of the Igneous Rocks. Vol. 3, The Intermediate Rocks:* Chicago (University of Chicago Press).

Kay, R. W., 1978. Aleutian magnesian andesites: melts from subducted Pacific ocean crust: *J. Volcanol. Geotherm. Res.*, 4:117–132.

Kikuchi, Y., 1888. Geological summary of the Bonin and Volcano islands. *Toyo Gakugei-zasshi*, 5:64–69. (In Japanese)

_____, 1890. On pyroxene components in certain volcanic rocks from Bonin Island. *J. Coll. Sci. Imp. Univ. Japan*, 3:67–89.

Kirkpatrick, R. J., 1978. Processes of crystallization in pillow basalts, Hole 396B, DSDP Leg 46. *In* Dmitriev, L., Heirtzler, J., et al., *Init. Repts. DSDP*, 46: Washington (U.S. Govt. Printing Office), 271–282.

Komatsu, M., 1980. Clinoenstatite in volcanic rocks from the Bonin Islands. *Contrib. Mineral. Petrol.*, 74:329–338.

Kuno, H., 1968. Differentiation of basalt magmas. *In* Hess, H. H., and Poldervaart, A. (Eds.), *Basalts* (Vol. 2): New York (Wiley), 623–688.

Kuroda, N., and Shiraki, K., 1975. Boninite and related rocks of Chichi-jima, Bonin Islands, Japan. *Rep. Fac. Sci. Shizuoka Univ.*, 10:145–155.

Kuroda, N., Shiraki, K., and Urano, H., 1978. Boninite as a possible calc-alkalic primary magma. *Bull. Volcanol.*, 41:563–575.

Kushiro, I., 1969. The system forsterite-diopside-silica with and without water at high pressure. *Am. J. Sci.*, 267A (Schairer Vol.): 269–294.

_____, 1972a. Effect of water on the compositions of magmas formed at high pressure. *J. Petrol.*, 13:311–334.

_____, 1972b. Determination of liquidus relations in synthetic silicate systems with electron probe analysis: The system forsterite-diopside-silica at 1 atmosphere. *Am. Mineral.*, 57:1260–1271.

_____, 1974. Melting of hydrous upper mantle and possible generation of andesitic magma: An approach from synthetic systems. *Earth Planet. Sci. Lett.*, 22:294–299.

Kushiro, I., and Sato, H., 1978. Origin of some calc-alkalic andesites in the Japanese Islands. *Bull. Volcanol.*, 41:576–585.

Lofgren, G. E., 1971. Spherulitic textures in glassy and crystalline rocks. *J. Geophys. Res.*, 76:5635–5648.

_____, 1974. An experimental study of plagioclase crystal morphology: Isothermal crystallization. *Am. J. Sci.*, 274:243–273.

_____, 1980. Experimental studies on the dynamic crystallization of silicate melts. *In* Hargraves, R. B. (Ed.), *Physics of Magmatic Processes:* Princeton (Princeton University Press), pp. 487–551.

Luth, W. C., Jahns, R. H., and Tuttle, O. F., 1964. The granite system at pressures of 4 to 10 kilobars. *J. Geophys. Res.*, 69: 759–773.

Macdonald, G. A., and Katsura, T., 1962. Relationship of Petrographic Suites in Hawaii: The Crust of the Pacific Basin. *Am. Geophys. Union Geophys. Mon.* 6: Washington (AGU), 187–195.

_____, 1964. Chemical composition of Hawaiian lavas. *J. Petrol.*, 5:82–133.

Meijer, A., 1980. Primitive arc volcanism and a boninite series: Examples from western Pacific island arcs. *In* Hayes, D. E. (Ed.), *The Tectonics and Geologic Evolution of Southeast Asian Seas and Islands*, American Geophysical Monograph 23: Washington (AGU), 271–282.

Mori, T., 1978. Experimental study of pyroxene equilibria in the system CaO-MgO-FeO-SiO_2. *J. Petrol.*, 19:45–65.

Mysen, B., and Kushiro, I., 1977. Compositional variations of coexisting phases with degree of melting of peridotite in the upper mantle. *Am. Mineral.*, 62:843–865.

Mysen, B., Kushiro, I., Nicholls, I. A., et al., 1974. A possible mantle origin for andesitic magmas: Discussion of a paper by Nicholls and Ringwood. *Earth Planet. Sci. Lett.*, 21:221–229.

Nakamura, Y., 1971. Equilibrium relations in Mg-rich part of the pyroxene quardrilateral. *Mineral. J.*, 6:264–276.

Natland, J. H., 1976. Petrology of volcanic rocks dredged from seamounts in the Line Islands. *In* Schlanger, S. O., Jackson, E. D., et al., *Init. Repts. DSDP*, 33: Washington (U.S. Govt. Printing Office), 749–777.

_____, 1978. Crystal morphologies in basalts from DSDP Site 395, 23°N, 46°W, Mid-Atlantic Ridge. *In* Melson, W. G., Rabinowitz, P. D., et al., *Init. Repts. DSDP*, 45: Washington (U.S. Govt. Printing Office), 423–445.

_____, 1980. Crystal morphologies in basalts dredged and drilled from the East Pacific Rise near 9°N and the Siqueiros Fracture Zone. *In* Rosendahl, B. R., Hekinian, R., et al., *Init. Repts. DSDP*, 54: Washington (U.S. Govt. Printing Office), 605–633.

O'Hara, M. J., 1965. Primary magmas and the origin of basalts. *Scot. J. Geol.*, 1:19–40.

Osborne, E. F., 1959. Role of oxygen pressure in the crystallization and differentiation of basaltic magma. *Am. J. Sci.*, 257:609–647.

_____, 1962. Reaction series for subalkaline igneous rocks based on different oxygen pressure conditions. *Am. Mineral.*, 47:211–226.

_____, 1979. The reaction principle. *In* Yoder, H. S., Jr. (Ed.), *The Evolution of the Igneous Rocks—Fiftieth Anniversary Perspectives:* Princeton (Princeton University Press), pp. 133–169.

Peacock, M. A., 1931. Classification of igneous rock series. *J. Geol.*, 39:54–67.

Petersen, J., 1891. Der Boninit von Peel Island. *Jahrb. Hamburgishen Wiss. Anst.*, 8:341–349.

Petersen, N., and Roggenthen, W. M., 1980. Rock- and paleomagnetism of Deep Sea Drilling Project Leg 54 basalts—East Pacific Rise and Galapagos Rift. *In* Rosendahl, B. R., Hekinian, R., et al., *Init. Repts. DSDP*, 54: Washington (U.S. Govt. Printing Office), 865–877.

Schmidt, R. G., 1957. Petrology of the volcanic rocks. *Geology of Saipan, Mariana Islands, Part 2. Petrology and Soils. U.S. Geol. Surv. Prof. Pap. 280-B:* Washington (U.S. Govt. Printing Office), 127–175.

Sharaskin, A. Ya., Dobretsov, N. L., and Sobolev, N. V., 1980. Marianites: The clinoenstatite-bearing pillow-lavas associated with the ophiolite assemblage of Mariana trench. *In* Panyiotou, A. (Ed.), *Ophiolites: Proceedings International Ophiolite Symposium, Cyprus, 1979:* Nicosia (Rep. Cyprus Min. Agric. Nat. Resources Geol. Surv. Dept.), 473–479.

Shiraki, K., and Kuroda, N., 1975. Boninite of the Bonin (Ogasawara) Islands. *Program Autumn 1975 Meeting Assoc. Mineral. Mining Geol. and Mineralogists, Petrologists, Economic Geologists in Japan, 55.* (In Japanese)

_____, 1977. The boninite revisited. *J. Geogr. Tokyo Geogr. Soc.*, 86:174–190. (In Japanese)

Shiraki, K., Kuroda, N., Maruyama, S., et al., 1978. Evolution of the Tertiary volcanic rocks in the Izu-Mariana arc. *Bull. Volcanol.*, 41: 548–562.

Shiraki, K., Kuroda, N., and Urano, H., 1977. Boninite: An evidence for calc-alkalic primary magma. *Kazan*, 22:257–261. (In Japanese)

Smith, J. V., 1969. Crystal structure and stability of the $MgSiO_3$ polymorphs: Physical properties and phase relations of Mg, Fe pyroxenes. *Mineral. Soc. Am. Spec. Pap.* 2:3–29.

Stark, J. T., 1963. Petrology of the volcanic rocks of Guam. *U.S. Geol. Surv. Prof. Pap. 403-C:* Washington (U.S. Govt. Printing Office), C1–C32.

Turner, F. J., Heard, H., and Griggs, D. T., 1960. Experimental deformation of enstatite and accompanying transformation of clinoenstatite. *Proc. 21st Int. Geol. Cong. Copenhagen*, 18:399–408.

Vogt, J. H. L., 1921. The physical chemistry and magmatic differentiation of igneous rocks. *J. Geol.*, 29:319–350.

Wager, L. R., and Brown, G. M., 1967. *Layered Igneous Rocks:* San Francisco (Freeman).

Walker, D., Shibata, T., and DeLong, S. E., 1979. Abyssal tholeiites from the Oceanographer fracture zone II. Phase equilibria and mixing. *Contrib. Mineral. Petrol.*, 70:111–125.

Wells, P. R. A., 1977. Pyroxene geothermometry in simple and complex systems. *Contrib. Mineral. Petrol.*, 42:109–124.

Wood, B. J., and Banno, S., 1973. Garnet-orthopyroxene and orthopyroxene-clinopyroxene relationships in simple and complex systems. *Contrib. Mineral. Petrol.*, 42:109–124.

Yoder, H. S., Jr., 1969. Calcalkalic andesites: Experimental data bearing on the origin of their assumed characteristics. *In* McBirney, A. R. (Ed.), *Proceedings of the Andesite Conference, Oreg. Dep. Geol. Miner. Ind. Bull.*, 65:77–89.

Yoder, H. S., Jr., and Tilley, C. E., 1962. Origin of basalt magma: An experimental study of natural and synthetic rock systems. *J. Petrol.*, 3:342–532.